CFD Analysis of Rudder Bulb Fins

Optimising a Marine Application Propulsion System through the development and implementation of Rudder Bulb Fins

Master Thesis

Matthew Cutajar
Thermal Energy and Process Engineering
May 2021

Aalborg University
Energy Technology

AALBORG UNIVERSITY
STUDENT REPORT

Energy Technology
Aalborg University
http://www.aau.dk

Title:
CFD Analysis of Rudder Bulb Fins

Theme:
Scientific Theme

Project Period:
Spring Semester 2021

Project Group:
Master Thesis

Participant(s):
Matthew Cutajar

Supervisor(s):
Chungen Yin

Copies: 1

Page Numbers: 56

Date of Completion:
May 28, 2021

Abstract:

The aim of this research project is to build upon previously established research in order to create a more robust CFD model of a marine application propulsion system, with a dedicated focus on establishing the optimal fin topology, through the investigation of various fin parameters and their influence on the propeller performance. The primary objective of this research is to design a rudder bulb fin geometry capable of augmenting the thrust generated while reducing energy losses, thus bettering the system performance. This is achieved by means of a two fin setup, both being oriented to optimally deal with the rotational inflow, reaching a system efficiency improvement of 4.99% over a system without any fins. Efforts to improve the system efficiency further through the use of multiple sets of fins, results in negligible increases in efficiency to the tune of 0.01%, which do not yield worthwhile improvements that are significant enough to warrant the cost of an extra set of fins.

Summary

The international shipping industry is responsible for 90% of global trade and yet despite contributing a moderate 2.2% of the worldwide CO_2 emissions, a more holistic approach is required. Regulatory bodies introduced in 2013 such as the Energy Efficiency Design Index (EEDI) and the Ship Energy Efficiency Management Plan (SEEMP), encourage the evolution of energy efficient technologies, furthering the visions of the Kyoto Protocol.

The aims and objectives of this research project are to build upon previous work in order to create an even better understanding of the effects of fin characteristics and establish an optimal topology capable of improving the generated thrust while also reducing energy losses. This is in parallel with the main focuses of the aforementioned mission statements of the aforementioned regulatory bodies.

A number of engineering principles are employed along with the features available in *Star-CCM+* in order to reproduce real conditions and scenarios, providing a more detailed insight. Since only the time-invariant behaviour is of interest, a steady state solver is used in conjunction with a segregated flow solver which evaluates the conservation equations and treats incompressible flows. The Navier-Stokes equations are solved by means of the SIMPLE algorithm. The SST $k - \omega$ turbulence model is used to model turbulent flow behaviour, while the transition SST model is used to predict the complex transitions between laminar and turbulent flows.

The control volume is modelled after a three-dimensional cylinder whose ends are bound by the Neumann conditions. The velocity inlet serves as a volume flux across the face while the pressure outlet imposes a working pressure on the face. Every other surface within the domain is constrained as a wall with a no-slip condition. The mesh is generated using tetrahedral cells and through the use of various *Star-CCM+* tools, one has full control over feature specific refinement, prism layers as well as cell growth rate. Therefore, a mesh of high quality and refinement may be created in order to accurately capture the necessary information and results.

A number of self-propulsion tests are performed to confirm the performance benefits of implementing a rudder bulb as well as to validate the computational setup against experimental data. Comparing both sets of results reveals a striking level of accuracy between the simulations and the experiments, thus verifying and validating the configuration of the continuum.

The optimisation of the propulsion system is achieved by first evaluating a base case, which also serves as a means of comparison against other developed geometries. A total of three sensitivity studies are performed, each corresponding to a fin characteristic thought to have significant potential in improving system performance. These are fin span, angle of attack and fin position.

The results of each sensitivity study are compiled into a final configuration which is tested below and above operating conditions in order to assess the performance during off-design instances. The final and best performing geometry comprises of a fin of length $0.06m$, an angle of attack of $5°$ relative to the rotational inflow, and is placed on the fixed part of the rudder bulb. This system boasts an efficiency of 74.84% which is just shy of a 5% improvement in efficiency over the base case without fins, whose efficiency is 69.85%.

This research project demonstrates the benefits of the developed optimised marine propulsion system which is able to recover energy losses while simultaneously augmenting the generated thrust in the most effective manner. The same approach and methodology can be applied to any case study and altered to suit different scenarios or system characteristics. The work done along with the results achieved, establishes a strong position for further research and detailed studies on energy saving devices and their advantages.

Preface

As part of the 10th Semester Study Curriculum for the Masters in Energy Technology at Aalborg University, students are required to write a thesis that delves into one of the many areas explored in the previous semesters.

This master thesis is conducted in partnership with MAN ES and is titled 'CFD Analysis of Rudder Bulb Fins'. The scope of this project is to investigate the flow around a marine application propulsion system and determine which ESD design variables are optimal for a reduction in power consumption.

Matthew Cutajar
mcutaj19@student.aau.dk

Aalborg University, May 28, 2021

Acknowledgements

I would like to express my sincere gratitude to my supervisor Chungen Yin whose guidance and support has been invaluable throughout this Master Thesis.

I would also like to extend my thanks to MAN es for hosting me at their offices, most especially Keun Woo Shin and Anders Ehlers, as well as the rest of the team for offering their expertise and insight on any challenges I encountered along the way.

Last but not least, I would like to convey my thanks to friends and family, especially the ones who have pushed me to strive to achieve better, by always believing in me.

Contents

List of Figures

List of Tables

List of Abbreviations

CFD Computational Fluid Dynamics

EEDI Energy Efficiency Design Index

ESD Energy Saving Device

ITTC International Tank Towing Conference

MRF Moving Reference Frame

RANS Reynolds Averaged Navier Stokes

SEEMP Ship Energy Efficiency Management Plan

SST Shear Stress Transport

Nomenclature

α	Angle of Attack	$^\circ$
η_o	Open water Efficiency	%
η_r	Adjusted propulsive Efficiency	%
Γ	Diffusivity Coefficient	m^2/s
γ	Intermittency	s
μ	Dynamic viscosity	Pas
μ_t	Turbulent viscosity	Pas
ν	Kinematic viscosity	m^2/s
ρ	Density	kg/m^3

C_D	Drag Coefficient	$-$
C_L	Lift Coefficient	$-$
D	Propeller diameter	m
J	Advance Ratio	$-$
K_Q	Coefficient of Torque	$-$
K_T	Coefficient of Thrust	$-$
n	Propeller rotational speed	rps
p	Pressure	Pa
Q	Torque	Nm
R_r	Rudder drag	N
T	Thrust	N
u^*	Frictional velocity	m/s
v_A	Free stream velocity	m/s
W_T	Weighting factor	$-$
y	Distance to nearest surface	m
y^+	Wall Distance	$-$

1 Introduction

The International Shipping Industry is recognised as one of the least polluting modes of global mass transport, conducing a moderate 2.2% of the worldwide amount of CO_2 emissions [1]. As the marine transportation sector continues to grow steadily, already being responsible for 90% of global trade, a more holistic approach is necessary to further improve its energy efficiency and emission control. Minor gains in efficiency or seemingly negligible reductions in fuel consumption translate into higher profit margins for businesses within the industry. This could allow companies to break into the market more successfully and develop a competitive edge that can be maintained, easily distinguishing them from the competition.

The Kyoto protocol recognises that the complex and large scale nature of the shipping industry makes it rather challenging to attribute emissions to one particular national economy. Therefore, reductions in shipping emissions are pursued in different avenues, such as the vessels themselves. Design advancements may be applied outside the commercial market, leisure craft such as large yachts and cruise ships may also benefit greatly. The driving forces in this sector are primarily the environmental mandates and the strive towards more efficient vessels that are able to perform at superior levels with lower operational costs.

The Energy Efficiency Design Index (EEDI), and the Ship Energy Efficiency Management Plan (SEEMP) are regulatory bodies that were introduced as of 2013 in order to encourage the evolution of energy efficiency technology. These bodies promote a number of technical measures aimed at encouraging the implementation of energy efficient equipment [2]. In theory, reducing the fuel consumption of vessels is something that can be achieved in a number different ways. This is commonly achieved by reducing the drag a vessel experiences. The flow of the fluid around the ship is by and large dictated by the hull design, therefore the appropriate amount of thought and attention should be invested into the optimisation of hull geometry.

Propulsion Systems are the main focus of development, since significant improvements in efficiency can be achieved. Apart from newer designs and vessels, optimised propulsion systems can be retrofitted onto old, existing vessels. This method is highly effective in boosting performance with limited capital expenditure. The combination of incremental improvements made to pivotal components of vessels together with constant research and development of various types of vessels paves the way for the introduction of new and innovative solutions, considerably enhancing ship performance.

1.1 Energy Saving Devices

Energy Saving Devices, commonly referred to as ESDs, are located in the aft of the ship, in the proximity of the propeller assembly. These auxiliary devices based on hydrodynamic interaction are intended to affect the conditions in and around the propulsion system in a favourable manner. The position of ESDs is categorised into the following three groups, as defined by Carlton [3] and as shown in Figure 1.1, each with its own unique flow characteristics. While it is clear that some devices transcend these boundaries, these zones serve more as a means to group similar devices.

- Zone I - Pre-Swirl zone: various thrust augmentation devices in the form of ducts, spoilers, fins and nozzles may be added for a direct benefit or to provide the propeller with a more advantageous flow by reacting with the final stages of boundary layer development over the stern of the ship.
- Zone II - Propeller Disc zone: energy saving devices in this region such as propeller boss cap fins are primarily intended to deal with the hull wake field, recovering energy which would otherwise be lost.
- Zone III - Post-Swirl zone: this region is strongly influenced by modifications made to the hull wake field, which occur as a result of the propeller slipstream. Rudder Bulbs, twisted rudders and additional thrusting fins are used in an attempt to recover energy which would otherwise be lost.

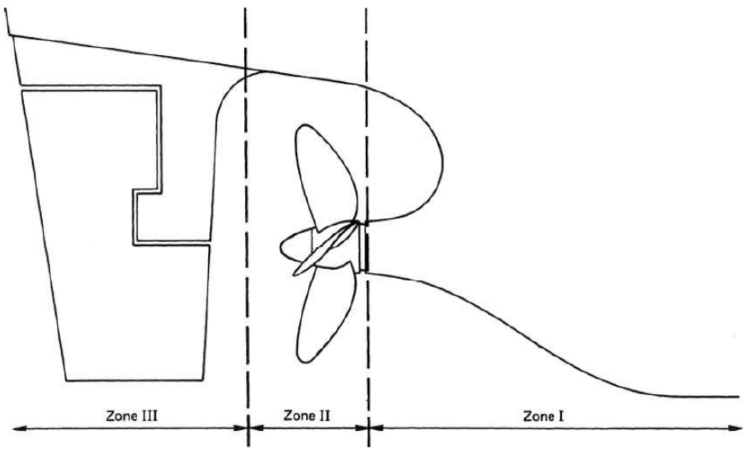

Figure 1.1: Classification Zones of Thrust Augmentation Devices [3]

Fitting multiple energy saving devices would not necessarily result in a cohesive system that produces a cumulative benefit. This is due to the fact that some devices mitigate flow regimes while others thrive upon them. Mutually independent devices may however be fitted to gain multiple benefits such as high efficiency gain with minimal capital expenditure. Furthermore, the lack of structural modification translates into ease of installation, making some ESDs extremely cost effective solutions for increasing propulsive efficiency.

1.2 Propeller Boss Cap Fins

Propeller hubs often experience strong vortices, which give rise to a loss in kinetic energy. This results in a reduction of the overall efficiency of the system. The adverse effects brought about by the aforementioned hub vortices can be alleviated with the introduction of propeller boss cap fins. These fins are commonly shaped like plates and are flat in design, while their height is dictated as a function of the propeller blade span - usually being around 10% of the blade span. The number of propeller blades gives an indication of how many fins should be used which are installed at a fixed pitch angle, relative to the propeller cone [3].

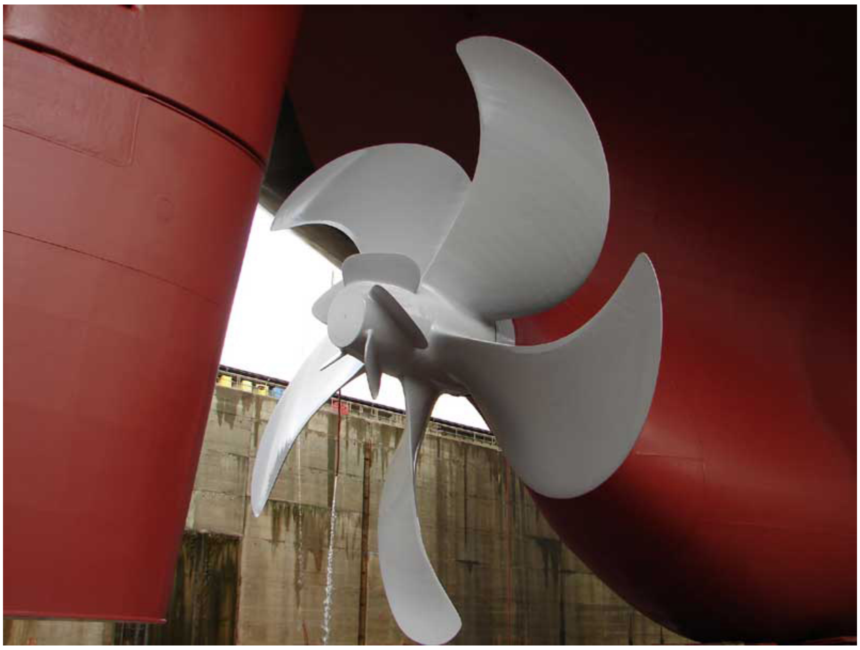

Figure 1.2: Propeller Boss Cap fins fitted onto propeller cone [4]

The working principle behind propeller boss cap fins, shown in Figure 1.2, is a simple one. Their purpose is to weaken the strength of the hub vortex, thus allowing the recovery of otherwise lost kinetic energy, while simultaneously contributing to an increase in propeller efficiency. Subsequently, through rectification of the incident flow with the rudder, cavitation is also alleviated.

Extensive research and testing has been carried out over the years with the intention of evaluating the flow measurements in the propeller wake. The results are encouraging, with various studies showing valuable gains in the open water efficiency of the propulsion system. Despite the presence of slight discrepancies between model-scale and full-scale implementations, investors have claimed to experience significant increases in propulsion efficiency of up to 10% through the integration of these fins [5].

1.3 Rudder Bulbs

The bulbous structures on the end of the rudder that extend to meet the propeller hub are aptly named rudder bulbs. The typical geometry of the said rudder bulbs is shown in Figure 1.3. The diameter of the bulb is intentionally limited to 40% of the propeller diameter to ensure a streamlined system. There are a number of benefits that a sleek and contoured design brings about, such as, a reduction in flow separation and decreased hub vortex generation. Apart from helping to alleviate cavitation on the rudder surface, rudder bulbs excel in mitigating contraction flow and negative pressure regions in the post-swirl zone [6].

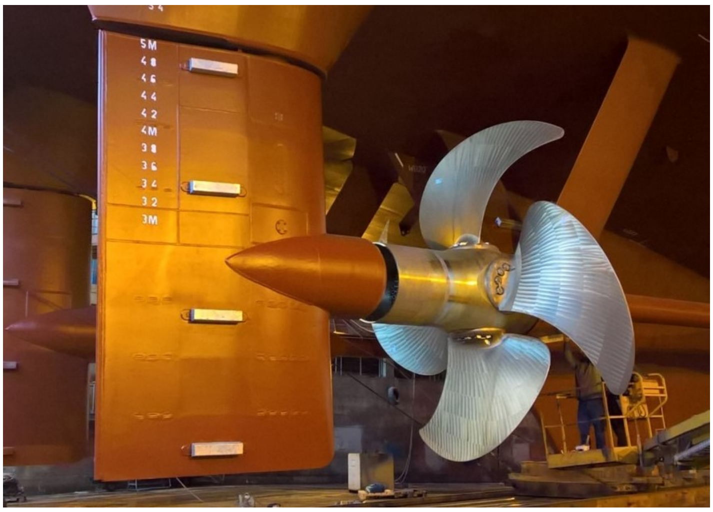

Figure 1.3: Rudder Bulb [7]

1.4 Rudder Bulb Fins

The performance of rudder bulbs may be further improved with the integration of fins in the form of aerofoils as can be seen in Figure 1.4. The number of fins as well as their arrangement is dependent on the requirements of the vessel. The primary goal of installing rudder bulb fins is to induce an additional lift force from the incident helical slipstream of the propeller. The horizontal component of the lift force translates into a forward thrust force, ergo augmenting the forward propulsion efficiency of the ship. Kawasaki Heavy Industries have tested a configuration of two aerofoils placed on the same horizontal plane, claiming to achieve reductions in propulsive power of up to 7% [8]. It is worth noting that rudder bulb fins are widely compatible, and can easily be integrated into systems with other ESDs.

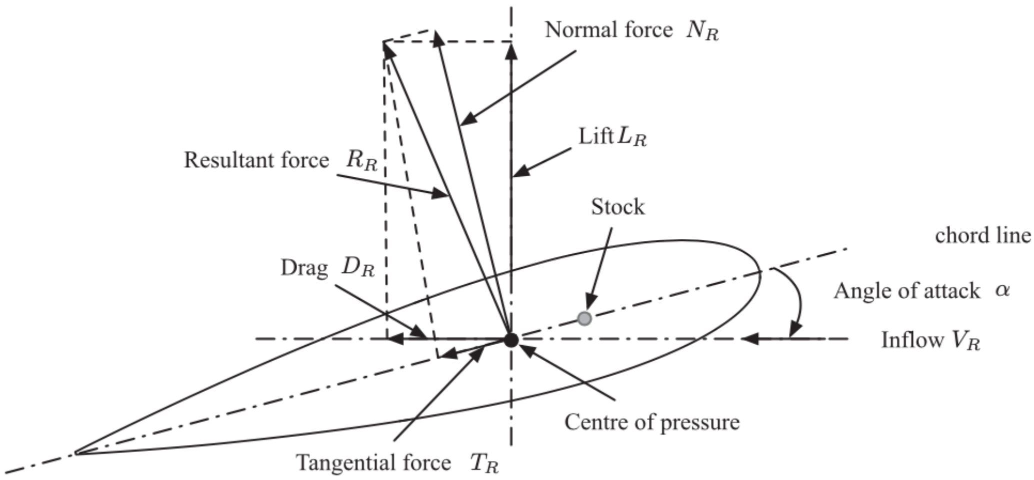

Figure 1.4: Rudder Bulb Fin Forces [9]

2 Problem Statement

The introduction of the Energy Efficiency Design Index in 2013, has meant that certain changes were implemented in an attempt to reduce the amount of CO_2 emissions. Energy Saving Devices are designed with the sole purpose of doing exactly that, making vessels much more efficient. Rudder Bulb Fins, which fall under the umbrella term of Energy Saving Devices, are found in the post-swirl region and can produce considerable enhancements.

This research project delves into the comprehensive design, analysis and optimisation of a Rudder Bulb Fin System through the use of commercial CFD software. The resulting simulations are validated through comparison with a reference simulation. The fins are carefully chosen so as to maximise the forward thrust force, and the optimal placement is determined in order to achieve the peak performance of the system. The benefits which rudder bulb fin systems are expected to bring about are:

- Streamlined propeller slipstream,
- Additional thrust generated on the fins,
- Reduced rudder drag and cavitation,
- Reduced suction pressure behind the propeller,
- Reduced hub vortex.

The aim of this analysis is to create a CFD model for the rudder bulb fins in order to facilitate the investigation of various fin parameters and their influence on the performance of the propulsive system. Furthermore, the optimal fin topology is determined, which is done through the study of the following design variables:

- Fin configurations,
- Fin length,
- Angle of attack,
- Number of fins.

2.1 Limitations

In order to precisely illustrate the extent of the effects of the design parameters of the fins, some assumptions have to be incorporated. All of the simulations are based exclusively on hydrodynamic principles, however, some aspects such as, added mass effects, slamming forces and cavitation are dismissed. This is not to say that such phenomena are insignificant when developing models of propulsion systems, however, they are omitted as they do not generate any thrust or reduce resistance.

3 Literature Review

This chapter aims to present a number of relevant published articles on the subject matter in a clear and concise manner, in order to summarise the findings of research and studies performed in the field. This section will follow a straightforward layout, wherein the explored research areas are discussed followed by a brief summary of their respective findings.

The simulations presented in the paper written by Shin & Andersen [10], aim to give a better understanding of efficiency gains during vessel manoeuvring. To facilitate a comparison of the benefits of a rudder bulb, two cases are simulated, one without and one with a rudder bulb. Gains in efficiency brought about by the integration of rudder bulbs are typically experienced at wide operational ranges. However, due to the rudder bulb being most streamlined with the fairing hub cap when it is in a neutral position, efficiency losses and cavitation remain serious issues at large rudder angles.

The front of the bulb and the hubcap are comprised of two concentric spherical surfaces, allowing for frictionless propeller rotation and rudder manoeuvrability with minimal clearance between the two. This is of course constructed within production capabilities of modern day shipyards. Figure 3.1 gives a pictorial representation of the interface geometry.

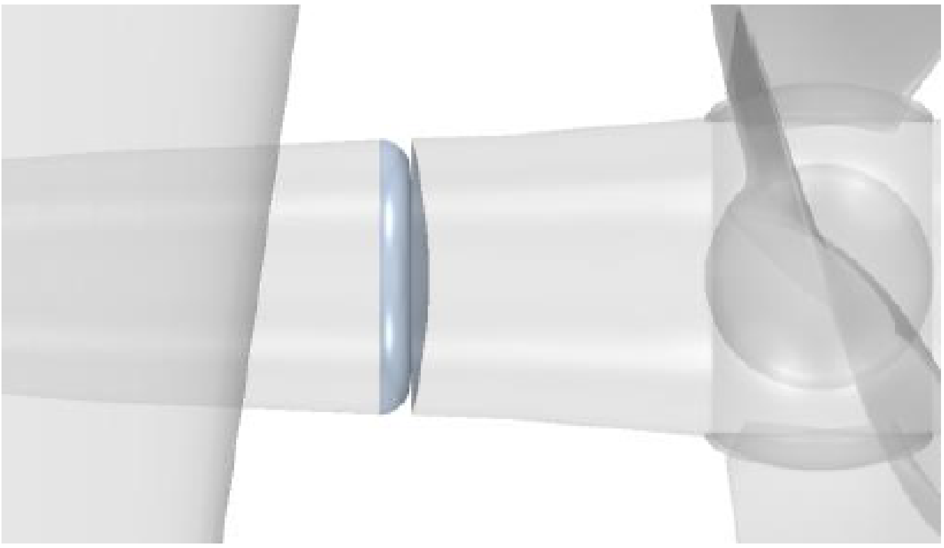

Figure 3.1: Side profile of the gap between the Bulb front and the propeller hub cap [10]

The efficiency improvements of the system can be accurately estimated by deriving an objective function that accounts for the excess thrust and the reduction in rudder resistance. The rudder bulb design considered for these simulations is intended for twin propeller craft whose hull wake region is considerably weaker when compared to single propeller vessels. It is for this reason that the hull wake region and the hull model itself are neglected for this study.

The propeller thrust increases noticeably while rudder resistance decreases simply with the introduction of a rudder bulb. Consequently, the self-propulsion point for a given ship speed is reached at a lower propeller speed. As a result, the total propulsive efficiency of the system is up to 6% higher with the integration of a rudder bulb. This considerable gain in propulsive efficiency is attributed to the major reductions in hub vortex losses and rudder bulb drag.

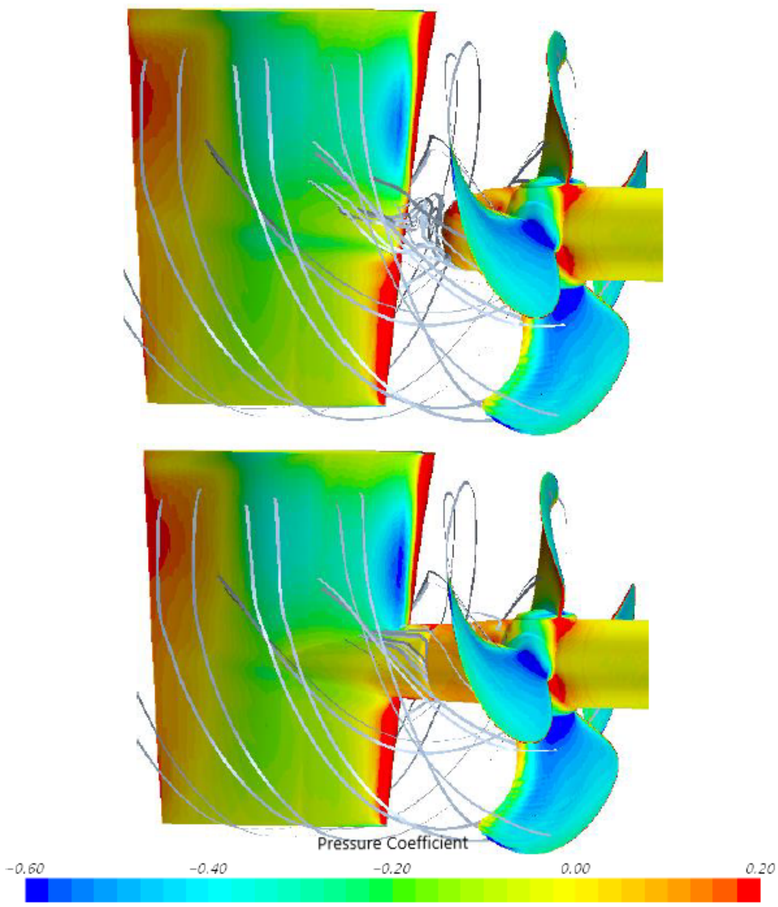

Figure 3.2: Streamlines and Pressure Coefficient on the propeller and rudder surfaces without and with the rudder bulb, from top to bottom, for a ship speed of 20kn [10]

Figure 3.2 offers a visual representation of the differences between the two simulations. The hub vortex is effectively eliminated by incorporating the rudder bulb into the geometry with no significant fluctuations in the pressure coefficient between the two cases.

In conclusion, Shin & Anderson established that the gains in efficiency are retained through a range of $\pm 10°$ from the neutral position of the rudder. The effectiveness of the rudder is also improved over the whole range of motion with the introduction of the rudder bulb. It is worth noting that these calculations are performed under open-water conditions and validated against experimental open-water test model data, which is often used to determine the hydrodynamic performance of a propeller.

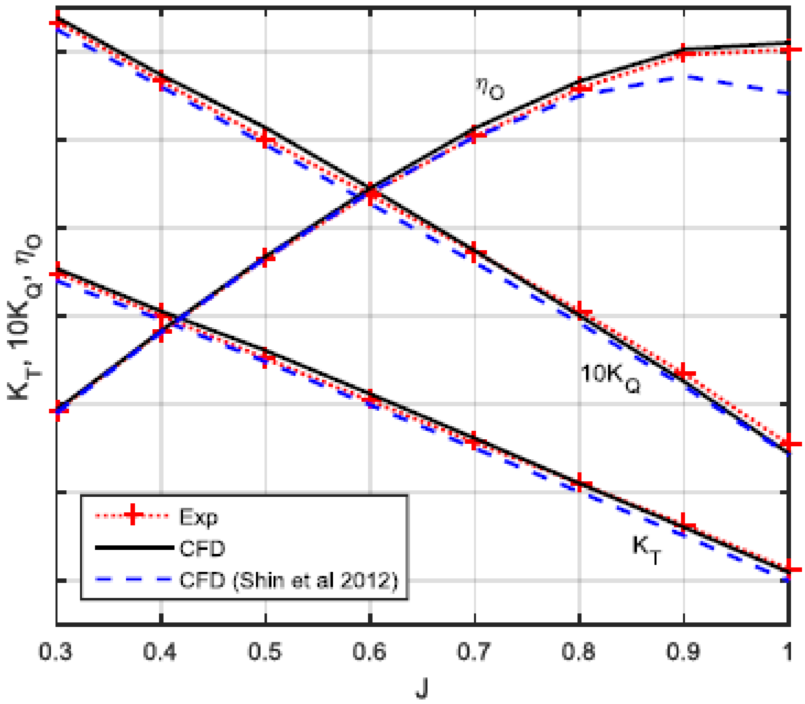

Figure 3.3: Experimental and CFD open-water curves [10][11]

Figure 3.3 illustrates the remarkable accuracy between the experimental data and CFD simulation results, where the three different plots represent the open water efficiency η_O, the coefficient of torque K_Q and the coefficient of thrust K_T, which are plotted over a range of advance ratios J. The simulations performed by Shin et al. exclude the use of transition models and reveal that η_O, K_T and K_Q are underestimated when compared to simulations that incorporate a transition model.

Another research paper written by Shin et al. [11] delves into the shape optimisation of rudder bulbs. As is common within these scientific journals, the objective is to minimise the necessary power required to propel a vessel forward at a desired ship speed. Therefore, using a complex heuristic optimisation algorithm created by Rao [12] enables the discovery of the optimum set of the following rudder bulb outer line variables; aft slope, characteristic diameter and fore slope.

The power reduction is defined as a function of the three aforementioned parameters, which allows for a more valuable insight into the shape optimisation of the rudder bulb. In order to accurately estimate fluctuations in power reduction, an objective function may be derived in terms of the thrust and efficiency improvements. The algorithm is initiated with 6 arbitrary design points, the worst of which is replaced with a new calculation within the considered range of parameters. This process is repeated for at least 100 iterations until the standard deviation of the objective function falls below 0.01.

It is evident from studying the streamlines and the pressure coefficient distribution plots from the simulations on the propulsion system components, that a hubcap geometry without a rudder bulb is exposed to a relatively higher risk of flow separation. The figures are characterised with several shades of red, verifying the negligible flow separation, yet reveal a very strong hub vortex, which is clearly shown in Figures 3.4a and 3.4b.

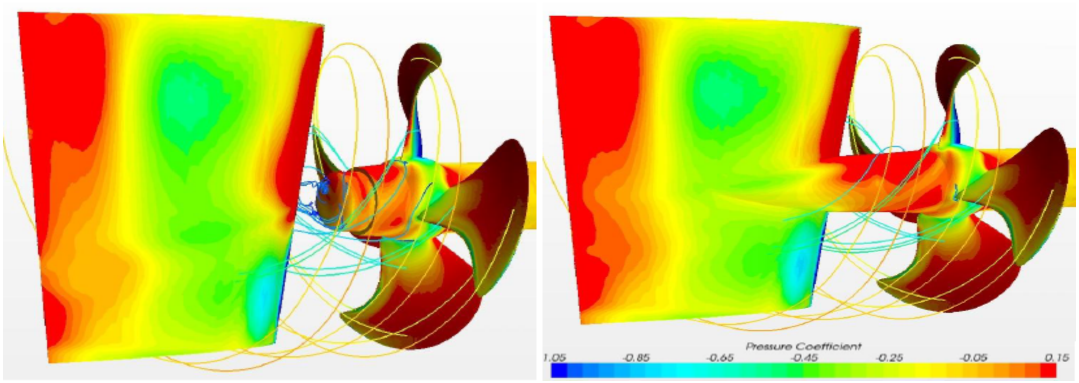

(a) Without Rudder Bulb **(b)** With Rudder Bulb

Figure 3.4: Starboard view of Streamlines and Pressure Coefficient behaviour on propeller and rudder surfaces [11]

The streamlined nature of the hubcap and the rudder bulb gives rise to a considerable decrease in rudder resistance. As a result, the rudder efficiency is increased, reducing the power by up to 2.5%. It is established that the clearance between the rudder bulb and the hubcap may be disregarded, since the results from simulations that model the gap, show no significant differences.

In order to garner an improved understanding of the rudder bulb performance, additional calculations are carried out for a range of ±2° of rudder rotation. This is of great relevance since when the rudder bulb in not in a neutral position, the flow around the steering margin may be critical. The rudder drag will always be greater when operating out of alignment with the hubcap. This is however, mitigated by means of the propeller thrust, which is enhanced with the addition of a rudder bulb. This occurs due to an intensified hub vortex as well as an increased loss in kinetic energy during operation at ±2° from the neutral rudder position. Figure 3.5 shows a bottom-up view of the propeller slipstream at an angle of 2° without and with a rudder bulb.

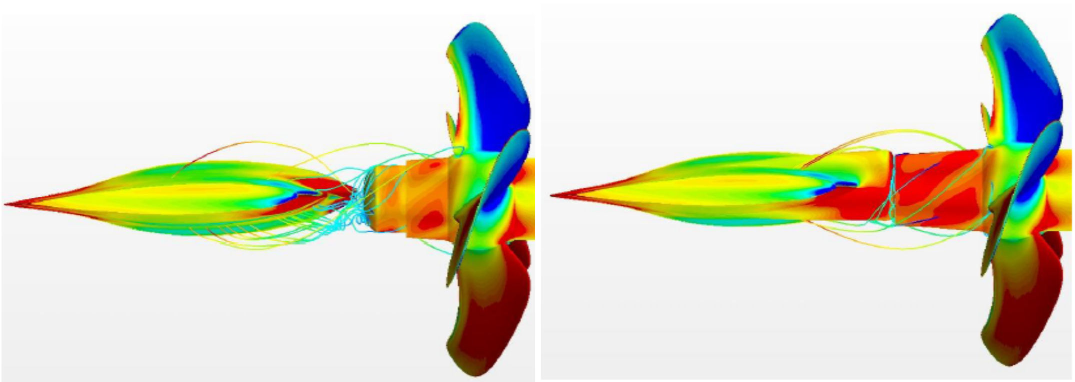

(a) Without Rudder Bulb **(b)** With Rudder Bulb

Figure 3.5: Streamlines and Pressure Coefficient distribution from the bottom of the rudder assembly [11]

Shin et al. conclude that geometry parameterisation and CFD based optimisation of rudder bulb systems generates further improvements in propulsion efficiency with power reductions of up to 5.7% and increased hull efficiencies of around 5.5%.

Rudder bulbs are designed in a way that minimises hub drag by reducing separation and decreasing pressure pulse, directly enhancing vessel propeller efficiency. Rubber bulb fins function in a similar manner, increasing the thrust in the rotational flow generated by the propeller to increase propulsive efficiency. The International Towing Tank Conference (ITTC) [13] held in 1999, specified that combining two or more energy saving devices on the same propulsive system could give energy gains between 4 and 14% at model scale. As fuel prices become more volatile and calls for greater environmental responsibility intensify, the amount of savings achieved by integrating ESDs is sufficient to incentivise further research and investment into rudder thrust fins.

Hai-long et al. [14] employ a numerical approach in order to explore the extent of the discrepancies between model scale simulations and full scale results. The research paper gives an insight into the effects of combining rudder bulbs with rudder thrust fins, which is directly related to the purview of this research project. Figure 3.6 depicts the system being tested, drawing the attention of the reader to the mesh refinement in areas of intricate geometry, which is purposely done to accurately capture all relevant information.

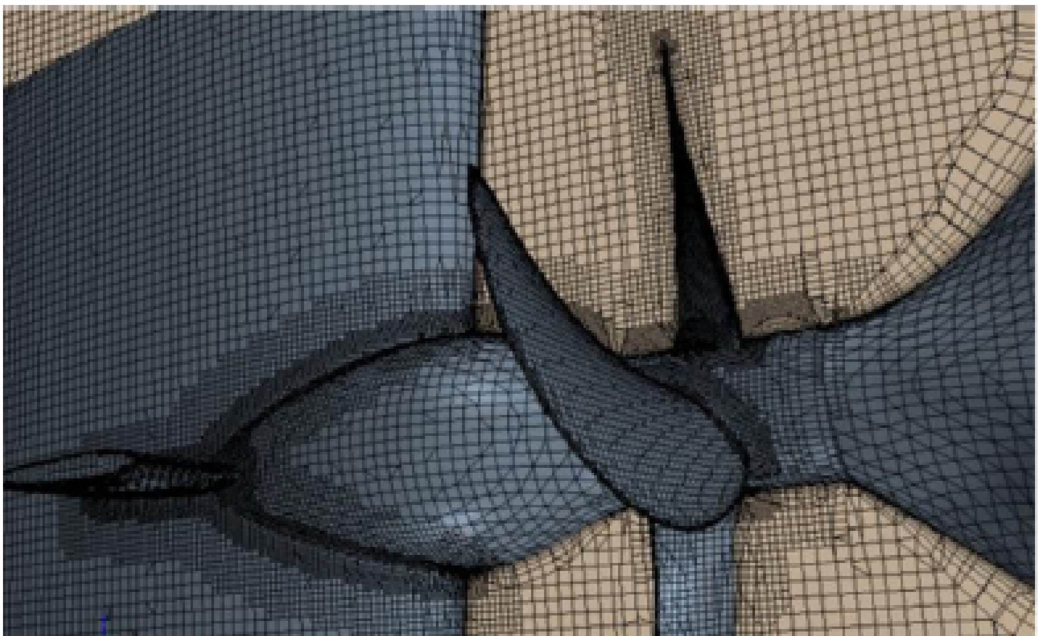

Figure 3.6: Generated Mesh for the combined ESD System [14]

The results reveal that a rudder bulb and fin assembly recover significant rotational and vortex losses, hence lessening the energy consumption. The rudder is responsible for the recovery of rotational losses while the vorticity is essentially eliminated due to the rudder bulb. Figures 3.7 and 3.8 give a better understanding of the differences in fluid flow and axial velocity between the two geometries.

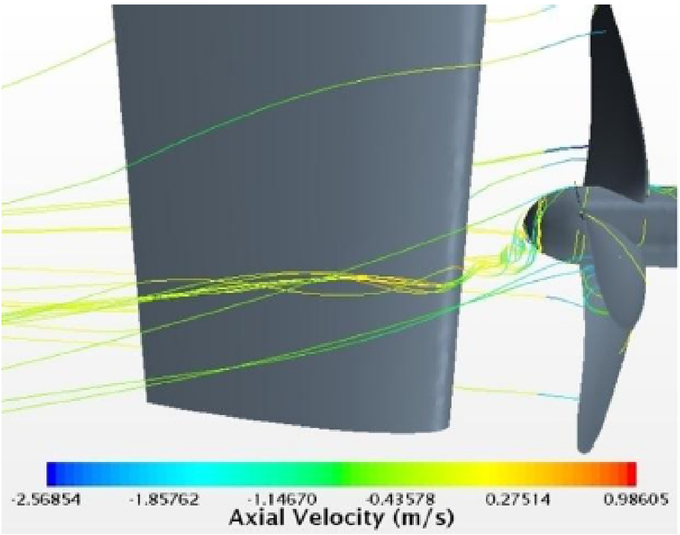

Figure 3.7: Starboard view of Streamlines and Axial Velocity profile on a conventional rudder [14]

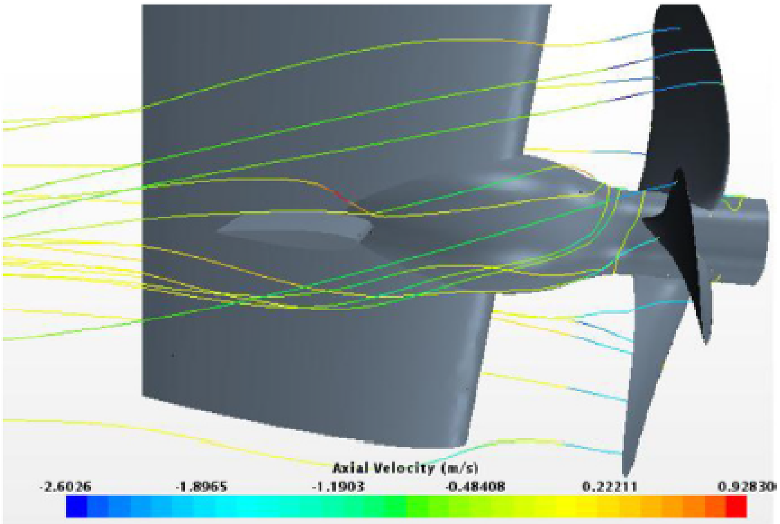

Figure 3.8: Starboard view of Rudder Bulb and Fin influence on fluid flow [14]

The influence of ESDs on the angular acceleration of the fluid flow at the stern of the craft can be further understood by accounting for the vorticity. The variation in vorticity may be interpreted as the result of fluid particle translation or unsteady flow, thus the fluctuation is referred to as angular acceleration. Figure 3.9 illustrates the vorticity magnitude profile.

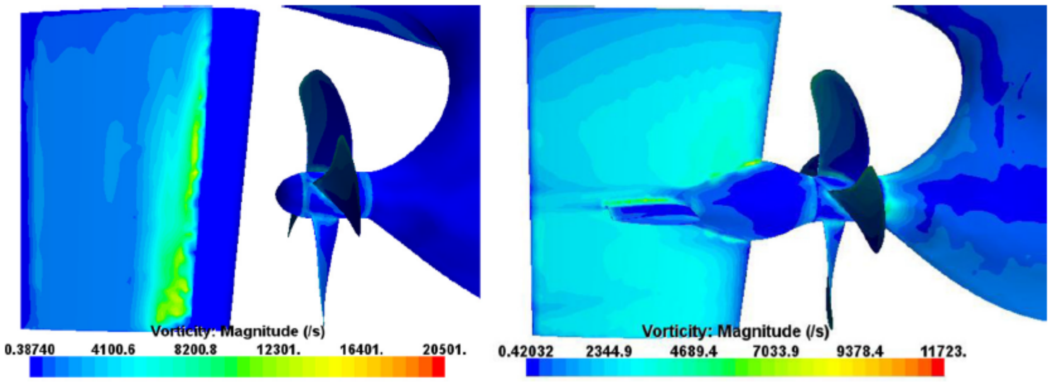

Figure 3.9: Influence of ESDs on vorticity magnitude [14]

A considerable shift in vorticity becomes evident when analysing the simulation with the rudder bulb fin assembly, wherein the magnitude is evenly distributed across the surface of the system. This may be strongly correlated to the recovery of rotational losses.

Hai-long et al. [14] concluded that CFD data calculated at model and full scale is comparable, with a simulated 4.8% gain in model scale propulsive efficiency, while full scale simulations showed improvements of 2.2%. The model scale propulsive efficiency is defined as the product of the open water, the relative-rotative and the hull efficiencies. Furthermore, the effects of ESDs on the flow in the post-swirl region, which are of great interest and relevance to this research project, inspire the necessary confidence for further development.

4 Methodology

This chapter is intended to give an insight into the engineering tools and techniques used within all the tasks and responsibilities of this research project. It outlines the necessary basics, giving the reader a much-needed foundation to be able to understand subsequent sections and chapters of this report.

4.1 Propulsive System Optimisation

Choosing the correct combination of ESDs is essential in order to maximise the system potential in terms of significant energy savings. The previous chapter, discussed extensively the effect of well designed and optimised rudder bulbs, which can increase the propulsive efficiency by up to 6%. Consequently, choosing the ideal rudder bulb geometry is no task to be taken lightly, especially when considering the integration of rudder bulb fins. This research project incorporates the previously presented geometry outlined by Shin et al. [11].

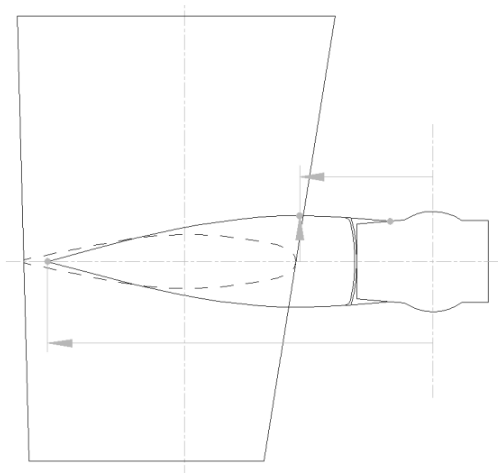

Figure 4.1: Vertical cross-section of a Rudder Bulb System [11]

Figure 4.1 depicts how the rudder bulb and the propeller hub geometries extended to meet one another. Upon closer inspection, one can observe a clearance between the two bodies whose purpose is to allow for vessel manoeuvrability. It is common practice, within the scientific journals discussed in the previous chapter, as well as many others, to neglect the steering margin - leading to unsophisticated models that are less resource intensive, both in terms of mesh as well as computational power.

4.2 Propulsive System Performance

Propeller designs are commonly measured based on the forces and moments they generate - which in an open-water environment, translate to the generated thrust and torque. The system efficiency may then be defined using the expressions established for the thrust and torque. In the interest of convenience, the results obtained from the simulations are expressed in dimensionless form, which are highlighted hereunder:

- **Advance Ratio** - defined as the ratio of the free stream velocity v_A, to the propeller rotational speed n and the propeller diameter D:

$$J = \frac{v_A}{nD} \tag{4.1}$$

- **Thrust Coefficient** - defined as a ratio of the generated thrust to the fluid density ρ, rotational velocity and propeller diameter:

$$K_T = \frac{T}{\rho n^2 D^4} \tag{4.2}$$

- **Torque Coefficient** - similar to the thrust coefficient, the torque coefficient is defined as the ratio of generated torque to fluid density, rotational velocity and propeller diameter:

$$K_Q = \frac{Q}{\rho n^2 D^5} \tag{4.3}$$

- **Open-Water Efficiency** - the derived expression makes use of the previous definitions to determine the propeller efficiency:

$$\eta_O = \frac{J K_T}{2\pi K_Q} \tag{4.4}$$

Performance plots are oftentimes a reliable guideline used to determine the optimal operating conditions of a vessel. However, since the thrust and torque coefficients are only applicable under free-stream conditions at a particular distance from the water surface, the performance results of real world applications may be misrepresented.

Generally speaking, it is good practice to evaluate entire systems that incorporate multiple devices in order to account for the effects of individual components. In this instance, when simulating the effects of a rudder bulb and rudder thrust fins, the additional hydrodynamic resistance generated by the rudder itself must be considered. Therefore, the expression used to determine the propulsive efficiency must be adjusted to account for the rudder drag as shown below:

$$\eta_r = \frac{(T - R_r)v_A}{2\pi n Q} \tag{4.5}$$

where R_r is the rudder drag. The main objective is to reduce power consumption by maximising thrust - since the change in net thrust and propulsive efficiency are both measures of propulsive performance, an objective function may be derived to accurately capture the reduction in power consumption:

$$f(X_i) = W_T \left(\frac{T_r(X_i)}{T_{r,ref}} - 1 \right) + \left(\frac{\eta_r(X_i)}{\eta_{r,ref}} - 1 \right) \tag{4.6}$$

where W_T is a weighting factor which is empirically determined. The net thrust and propulsive efficiency are defined by $T_r(X_i)$ and $\eta_r(X_i)$ respectively, while $T_{r,ref}$ and $\eta_{r,ref}$ represent the reference values.

4.3 Open Water Testing

The estimation of ship propulsion coefficients is extensively facilitated by means of open water tests. These tests are often performed using stock propellers or even scaled models of the actual propellers to be fitted to the vessel. The purpose of these model-scale tests is to obtain a better understanding of the behaviour of the actual propellers. Figure 4.2 shows the experimental set up, wherein the model is fitted to a horizontal driveshaft on a streamlined airfoil section strut. The assembly is pushed forward with the propeller ahead of the housing so that it is effectively in an undisturbed water.

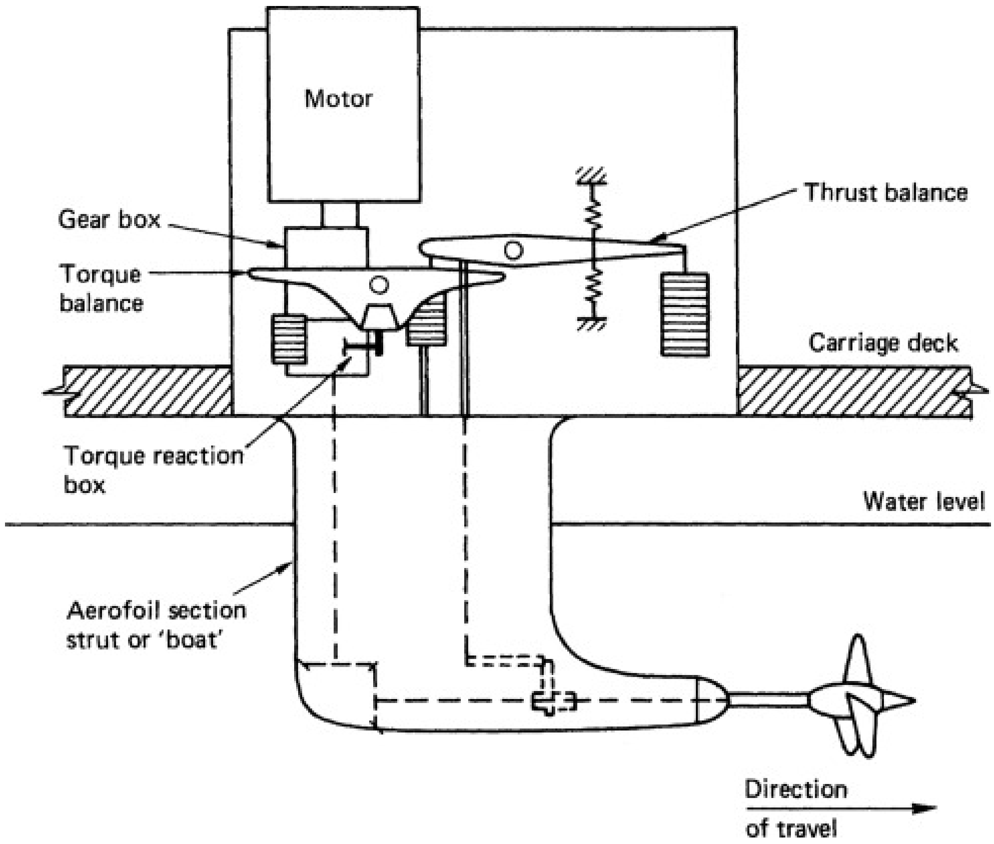

Figure 4.2: Open water propeller test using a towing tank carriage [3]

The thrust and torque values are measured at distinct intervals for various carriage speeds and propeller revolutions. Usually, the recorded values are amended experimentally to account for the hub resistance. The thrust and torque results are tabulated in dimensionless form as discussed previously. One of the great advantages of open water tests is the elimination of cavitation effects.

The open water test results exclude the influence of a hull wake, therefore an allowance should be factored in to more accurately represent the real flow conditions a particular design will be subjected to when operating behind the hull it drives. Implementing hull wake effects into simulations would significantly increase the processing time and computational power needed, thus open water conditions are chosen in the interest of simulation complexity and time management.

5 Modelling

This chapter explores the various tools and techniques used in *Star-CCM+*, to create successful models within all engineering disciplines. *Star-CCM+* is a complete multi-physics solution designed to capture physical phenomena affecting the performance and longevity of equipment and machinery during their operational life. Reproducing real world conditions and scenarios may be achieved easily, offering a more detailed insight.

5.1 Governing Equations

The fluid flow in and around an arbitrary body may be accurately represented by means of the following differential governing equations:

- Continuity Equation:

$$\frac{\partial(\rho \overline{u}_i)}{\partial x_i} = 0 \tag{5.1}$$

- Momentum Equation:

$$\frac{\partial(\rho \overline{u}_i)}{\partial t} + \frac{\partial(\rho \overline{u}_i \overline{u}_j + \rho \overline{u_i' u_j'})}{\partial x_j} = -\frac{\partial \overline{p}}{\partial x_i} + \frac{\partial \overline{\tau_{ij}}}{\partial x_j} \tag{5.2}$$

- Mean viscous Stress Tensor:

$$\overline{\tau}_{ij} = \mu \left(\frac{\partial \overline{u}_i}{\partial x_j} + \frac{\partial \overline{u}_j}{\partial x_i} \right) \tag{5.3}$$

- Reynolds Stress Tensor:

$$\rho \overline{u_i' u_j'} = \mu_t \left(\frac{\partial u_i}{\partial x_j} + \frac{\partial u_j}{\partial x_i} \right) \tag{5.4}$$

where ρ denotes the fluid density, p represents the pressure, μ is the dynamic viscosity, μ_t is the turbulent viscosity and - $\rho \overline{u_i' u_j'}$ is the mean Reynolds stress tensor.

The turbulent or eddy viscosity is determined using either the $k-\omega$ model or the $k-\epsilon$ model, depending on which one is used. The expressions defined above are transformed into a system of linear equations using the finite volume method, making simulations less computationally taxing. The system of governing equations is then solved over a continuous spatial domain partitioned into a number of cells, while the time domain is given an analogous treatment.

The above set of equations is discretised into a system of linear algebraic equations to deduce the general transport equation:

$$\underbrace{\frac{\partial(\rho\phi)}{\partial t}}_{Transience} + \underbrace{\nabla(\rho u\phi)}_{Convection} = \underbrace{\nabla(\Gamma_\phi \nabla_\phi)}_{Diffusion} + \underbrace{S_\phi}_{Source} \tag{5.5}$$

where ϕ represents the variable in question and Γ is its diffusivity coefficient. The terms in the general transport equation are, from left to right:

- Transient term - Accumulation of ϕ within the control volume;
- Convective term - Net rate of flow of ϕ out of the element;
- Diffusive term - Rate of increase of ϕ due to diffusion;
- Source term - Variation of ϕ due to additional sources or sinks.

5.2 Solvers

The aim of the simulations is to determine the steady state, time invariant behaviour of the system - therefore a steady state solver is used. Meanwhile, the segregated flow solver, which evaluates the conservation equations sequentially, is chosen to treat incompressible flows.

Furthermore, a pressure-velocity coupling algorithm together with a pressure correction equation are used in order to satisfy the general transport equation for a particular velocity field. This is achieved by using the SIMPLE algorithm, which is a widely used numerical method to solve the Navier-Stokes equations.

5.3 Turbulence Modelling

The Reynolds Averaged Navier Stokes (RANS) equations are commonly used for modelling turbulent flow behaviour. The principle behind the equations, is referred to as the decomposition of the flow variable, whereby an instantaneous quantity is decomposed into a time averaged (mean) and fluctuation component.

$$\phi = \overline{\phi} + \phi' \tag{5.6}$$

The Shear Stress Transport (SST) $k-\omega$ turbulence model employs both the $k-\omega$ model near walls and the $k-\varepsilon$ within the free stream. The $k-\omega$ model functions best in the inner region of the boundary layer revealing the behaviour of the viscous sub-layer, while the $k-\varepsilon$ model is used in free shear flow, predicting the flow behaviour away from walls. This hybrid combination of appropriate blending functions ensures that the correct one is used throughout the entire flow field.

The SST $k-\omega$ turbulence model:

- employs the shear stress limiter to prevent the excess build up of turbulent kinetic energy near stagnation regions,
- is less susceptible to flow variations outside boundary layers when compared to other models.

5.4 Transition Model

Predicting the transitions between laminar and turbulent behaviour within fluid flows is a complex area of CFD that is still not yet fully understood. Transition models are dedicated to predicting where and when this change happens, however, simulating the interaction between laminar and turbulent regions is oftentimes case specific, making it all the more challenging.

The transition SST model is the more established approach of two, predicting the shift between laminar and turbulent flows by combining the SST $k-\omega$ transport equations with another two extra transport equations. The first equation functions as a measure of the intermittency γ, which represents the period of time the flow has spent in a fully turbulent state. Meanwhile, the second equation is a transport equation used to determine the transition onset criteria in terms of the momentum-thickness Reynolds number. This model is far superior to the less common turbulence suppression model.

This model is far superior to the less common turbulence suppression model. Based entirely on user input - it resolves no equations, relying entirely on the ability of the user to define locations of transition. Its lack of mathematical nature makes it insufficiently robust, yet despite its low computational cost, remains an unreliable tool for the prediction of transition.

5.5 Boundary Conditions

In order to accurately define the control volume, a number of boundary conditions that constrain the continuum must be established. The control volume is fashioned as a three dimensional cylinder, with the face where the flow is first incident being set as a velocity inlet, while the opposite end of the control volume is defined as a pressure outlet. The boundaries are constrained by the Neumann conditions, where the velocity inlet condition serves as a volume flux across the face, and the pressure outlet condition introduces a working pressure on the face, where the static pressure is defined as the ambient pressure. Every other part within the domain is constrained as a wall with a no-slip condition, which essentially translates to the boundary layer development on said surfaces.

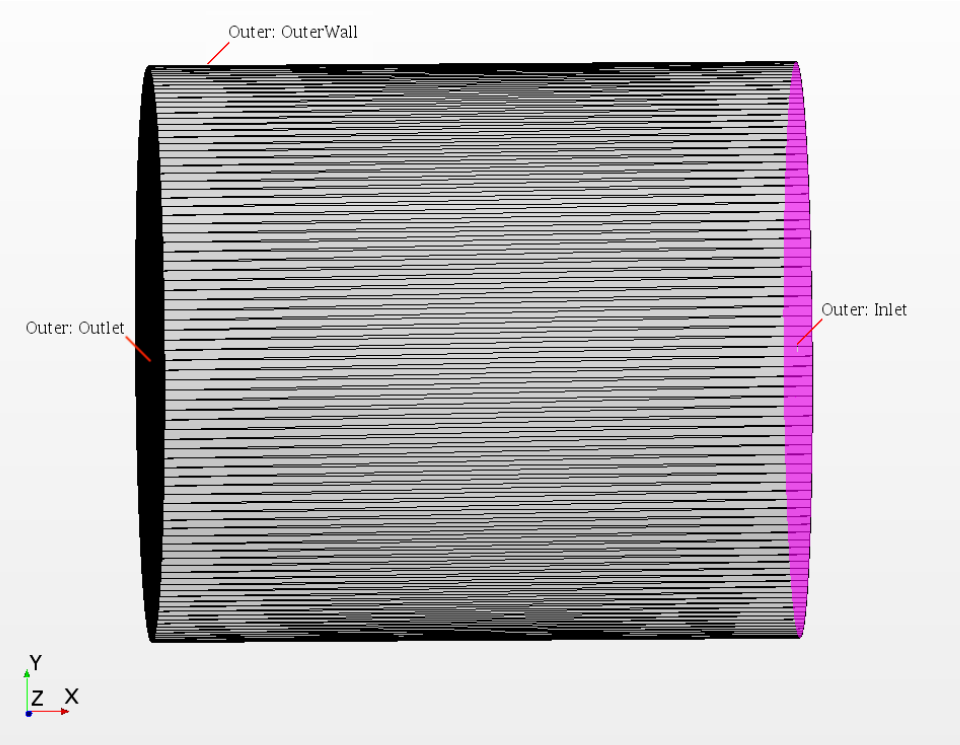

Figure 5.1: Boundary Conditions for the Computational Domain

5.6 Meshing

Star-CCM+ offers a wide variety of meshing tools, enabling the users to generate a mesh of excellent quality. Oftentimes, when dealing with imported geometries of inadequate quality, the surface wrapper is used to compensate for any holes, gaps or intersecting surfaces. The surface remesher can then be applied to re-triangulate closed surfaces, creating a flawless geometry which allows a volume mesh to be generated. Volume meshes can be generated in numerous ways, ultimately the preference of model for the core volume mesh is dependent on the:

- geometry thickness,
- mesh surface quality,
- amount of computational power available,
- convergence rate and desired solution accuracy.

The cells that constitute a volume mesh can take one of three forms - tetrahedral, polyhedral or hexahedral cells, all of which have their own features and characteristics. The trimmer mesh tool is commonly used when dealing with geometries of varying complexity, providing a robust and efficient means of developing a fine mesh with minimal cell skewness, while allowing for surface quality independence as well as a number of refinement options. Furthermore, the trimmer enables the user to define prism layers, with full control over variables such as cell growth rate and other feature specific refinement. This level of control along with the ability to define ultra-fine regions allows for highly accurate simulations. Figure 5.2 shows the prism layers on the leading edge of a propeller blade.

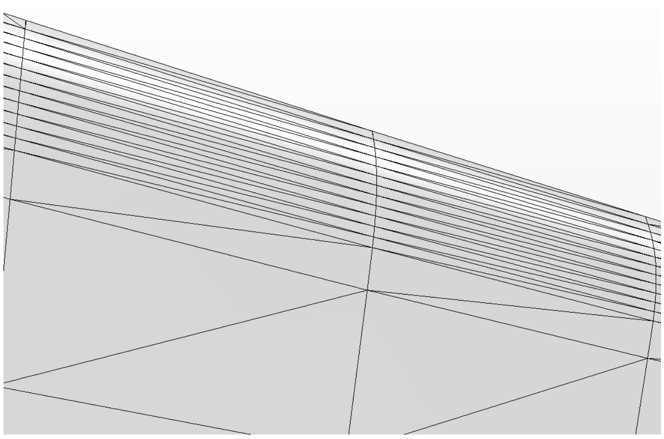

Figure 5.2: Prism Layers at a Propeller Blade Leading Edge

5.7 Wall Distance

Mesh Quality becomes increasingly important when resolving the turbulence at near-wall regions due to its sensitivity. Propeller blade surfaces experience sudden changes from a no-slip condition to free stream conditions as a result of damping of normal wall components and the production of turbulence due to shear. Understanding the flow behaviour in and around these regions is critical and can be facilitated with the use of the y^+ value.

In addition, forces such as the thrust and the torque are the primary concern of this research, thus in order to accurately predict these forces, a fine mesh well resolving the boundary layers on the wall surfaces is a must.

The y^+ value is a dimensionless entity introduced to obtain the height of the first cell within the mesh near a wall or surface. Combining the y^+ value together with a mesh growth rate allows for a true representation of information without an overly refined mesh. The expression for y^+ is given as:

$$y^+ = \frac{u^* y}{\nu} \tag{5.7}$$

where u^* is the frictional velocity at the surface, y is the distance to the nearest surface and ν is the kinematic viscosity of the fluid. The three layers defined by the wall distance are:

- Viscous sub-layer - $(0 < y^+ < 5)$,
- Buffer layer - $(5 < y^+ < 30)$,
- Inertial sub-layer - $(30 < y^+ < 300)$.

The viscous sub-layer is characterised by negligible amounts of turbulence while the inertial sub-layer is fully turbulent and experiences no viscous effects. The buffer layer consists of both viscous and turbulent effects, making it impractical for computational purposes. The viscous sub-layer is commonly used due to its higher accuracy over the inertial sub-layer.

5.8 Moving Reference Frames

The rotation of the propeller must be accounted for in order to accurately represent the behaviour of the fluid flow around the propulsive system. Portraying the rotational nature of such parts in an authentic manner is an arduous task, hence Moving Reference Frames (MRF) are used to approximate the constant rigid motion. This method provides an analysis of the time-averaged behaviour rather than a time-accurate solution.

Obtaining a time-averaged result is achieved by mimicking the fluid rotation along an axis, parallel to the direction of the inlet. Then, the flow variables can be transferred through the interface between the stationary and moving parts of the mesh. Alternatively, producing a transient solution shows negligible gains in accuracy with significantly higher needs for computational power, making the MRF approach far superior.

5.9 Monitors

Recording and storing data from a simulation while it is running is particularly useful when presenting results in the form of graphs or plots. Monitors provide a mechanism that facilitates, in this case, sampling the two parameters of interest, the thrust and torque. The thrust is found by multiplying the sum of the pressure and shear forces by a direction vector. Similarly, the sum of pressure and shear forces is multiplied by distance from the axis of rotation to obtain the torque monitor.

Monitoring the physical parameters of interest in the simulation is one of the key measures used to ensure convergence in this study. Furthermore, the thrust and torque figures are also used as a means of verification and validation against experimental data, thus documenting them for later access is vital in ensuring the success of this research.

6 Results

Establishing a reference point for the rudder bulb fin simulations is necessary in order to serve as a means of comparison against a base line, especially since no experimental data is available. A number of preliminary simulations are also performed in order to verify the configuration of the mesh by validating the results against established experimental data.

6.1 Mesh Quality Specifications

The mesh continuum is defined in a particular manner that allows for a Moving Reference Frame within the domain. The proportions of the cylindrical fluid domain are defined in terms of the propeller diameter, with the length of the cylinder measuring $10D$ and the radial dimension being $4D$. At a $0.1D$ offset, upstream of the centre of the fluid domain, the propeller geometry is housed within an MRF that measures $3D$ axially and $0.7D$ radially. A buffer region between the propeller geometry and the interface is accounted for in order to accurately capture the flow in and around the propeller itself.

Table 6.1: Mesh Quality details

	Inner Mesh	Outer Mesh
Max. Cell Size	0.02m	0.033m
Prism Layers	10	10
Prism Layer Stretching	1.2	1.2
Prism Layer Thickness	2.04×10^{-4}m	2.04×10^{-4}m
Growth Rate	1.2	1.1

The quality of the mesh is specified in further detail in Table 6.1, offering a much better understanding of the attention to detail and refinement that ultimately captures the necessary results. The cylindrical geometry that encapsulates the propeller itself is referred to as the Inner Mesh, while the cylinder surrounding the entire propulsive system is referred to as the Outer Mesh. The cell count of such a mesh is approximately 28 million.

The surface mesh is comprised of triangular cells, thus it follows that the volume mesh is generated using tetrahedral cells, however, the surface mesh is treated using the surface remesher while the trimmer is applied to the volume mesh. An essential tool that allows the accurate capture of wall bounded flow phenomena is the prism layer meshing feature, which is used to refine the cells adjacent to wall boundaries. The mesh is presented in its final form in Figure 6.1.

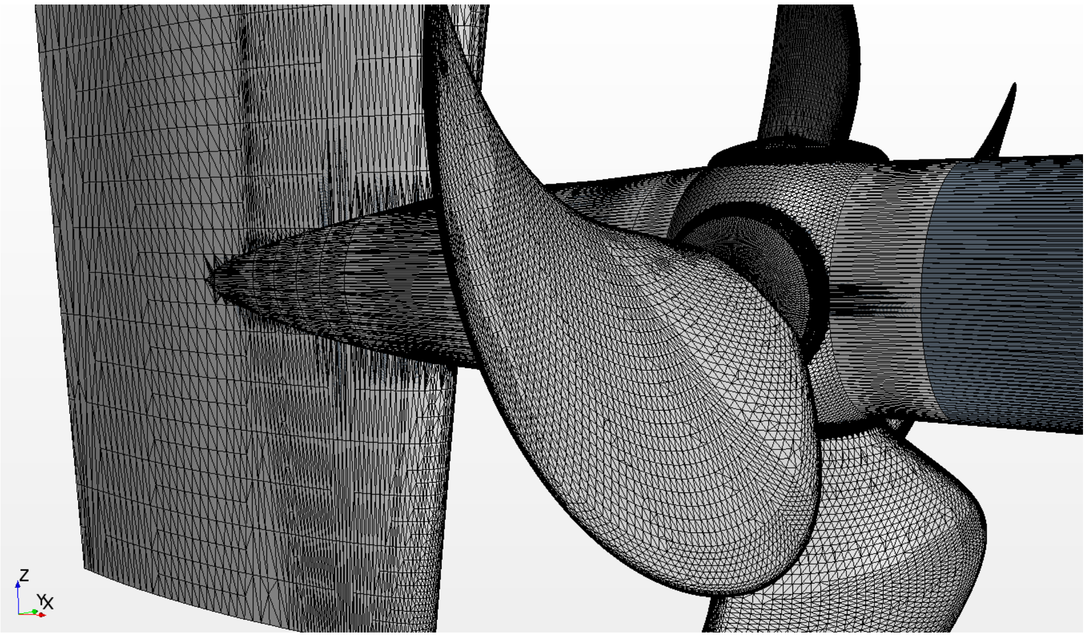

Figure 6.1: Geometry Surface Mesh for base case

The relationship between the advance ratio, free stream velocity and the rotational speed is defined in Equation 4.1 in Chapter 4. Following the strict correlation between the three variables, the fluid velocity at the inlet is constrained as a uniform flow field that corresponds to the current advance ratio. The opposite end is defined as a pressure outlet, imposing a working pressure on the face. All other surfaces within the domain are defined as walls with no-slip conditions.

The turbulence intensity within the free stream is another defining characteristic which is modelled using an under-relaxation factor of 0.8, ensuring a more stable solution process. Furthermore, any physical properties pertaining to the fluid domain such as the viscosity and the density assume the values of water.

6.1.1 Wall Distance

In order to ascertain that the results produced are an accurate and true representation, without the use of an overly refined mesh, the wall distance is checked and analysed by means of a plot similar to the one presented in Figure 6.2. The colour plot clearly shows the distribution of the y^+ distance mapped onto the geometry. It is evident that the y^+ value does not exceed 5 anywhere, thus the simulations are performed within the viscous sub-layer.

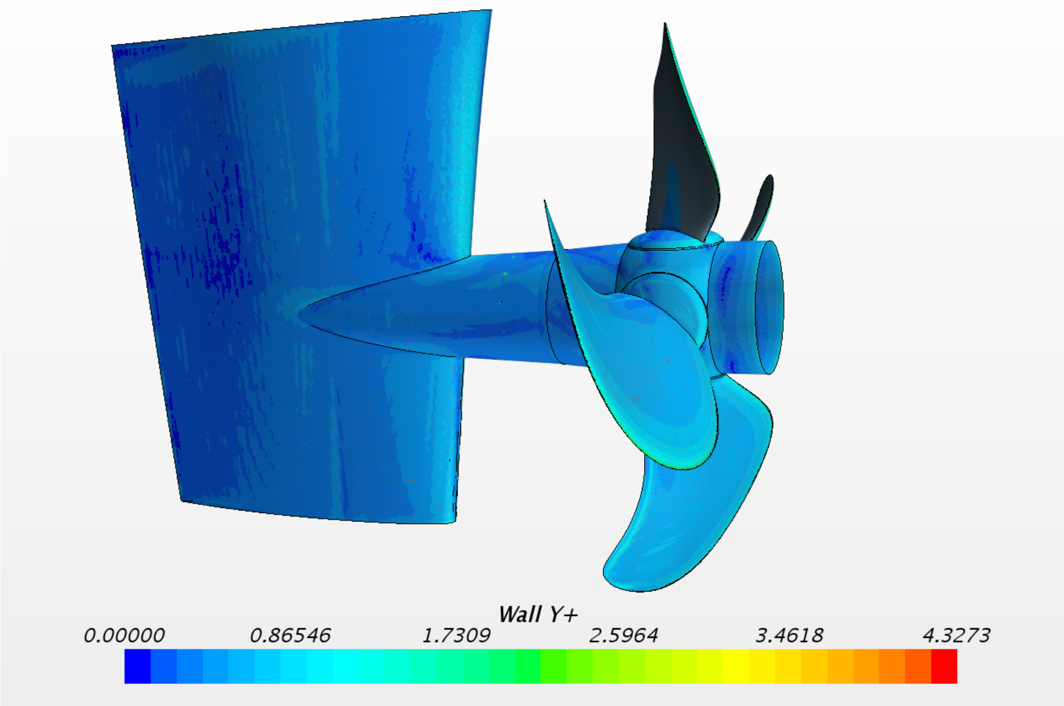

Figure 6.2: Wall Distance y^+ mapped onto Geometry

The trend of low y^+ values is unwavering, even when testing geometries with rudder bulb fins. The span of the fins cannot exceed the propeller radius as this would introduce new issues, most specifically manoeuvrability, thus it is logical that any fin geometry appended to the already tested geometry will have a maximum y^+ value that is less than that of the tip of the propeller blades.

The aforementioned results may also be presented in the form of a histogram, such as the one in 6.3, which may be beneficial in understanding the distribution of y^+ values.

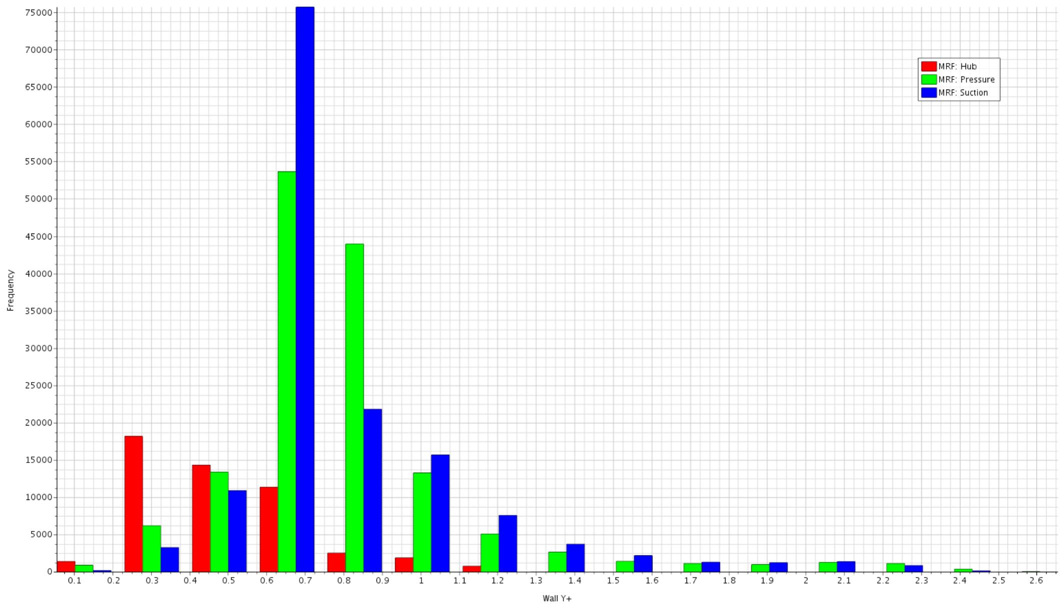

Figure 6.3: Wall Distance y^+ Histogram

Upon further inspection, the histogram reveals that the majority of the cells within the MRF have a y^+ value of 1 or less, thus the simulation is well within the viscous sub-layer. The high frequency of the y-axis is owed to the resolution of the mesh, since the mesh is further refined, the frequency is rather quite large.

6.1.2 Residual Convergence

The simulations are all performed at a ship speed of $20knots$, which translates to a propeller rotational speed of $9.96rev/s$ and an advance ratio of 0.9129. The maximum number of iterations for one such case is 1500, as the residuals converge and tend to oscillate around a mean value toward the later stages of solution convergence. Although 1500 iterations may seem insufficient to reach proper convergence or results that bare any significance, comparisons against experimental data prove otherwise. The mesh configuration along with the level of residual convergence is more than enough to achieve a striking level of accuracy between computational and experimental results.

A number of substantial changes are applied to the setup in the previously published work. The previous configuration showed residuals that decreased by one order of magnitude. In order to mitigate this issue, a number of test simulations were performed on the plain propulsion system geometry in pursuit of better convergence.

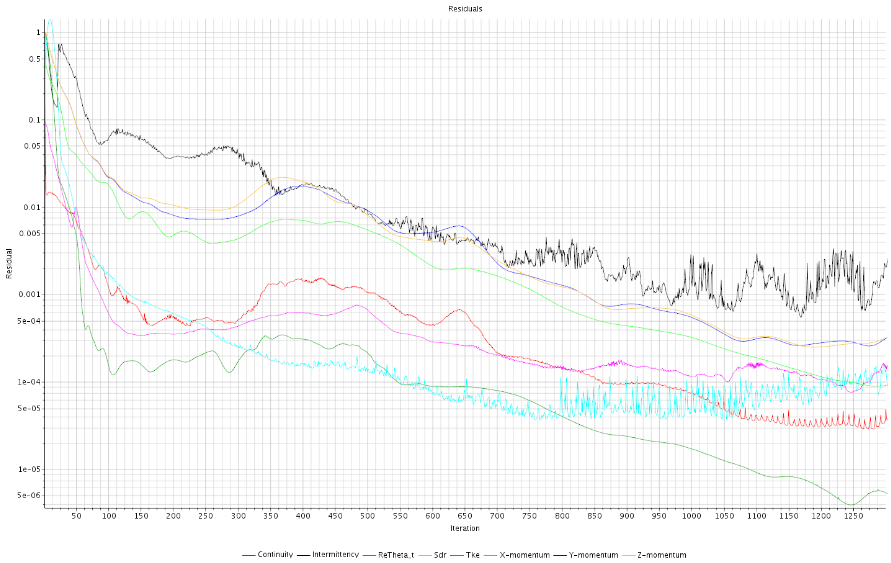

Figure 6.4: Solution Convergence as a Function of Iterations

Observing Figure 6.4 reveals that the residuals decrease by at least three orders of magnitude. Analysing the plot further one may observe an initial instability within the first 50 iterations, which is later resolved as the solution reaches convergence. This significant improvement of residuals is achieved by means of two important changes to the continua; the segregated flow solver being changed to first order from second order and a number of mesh refinements that are applied to both the inner and outer meshes.

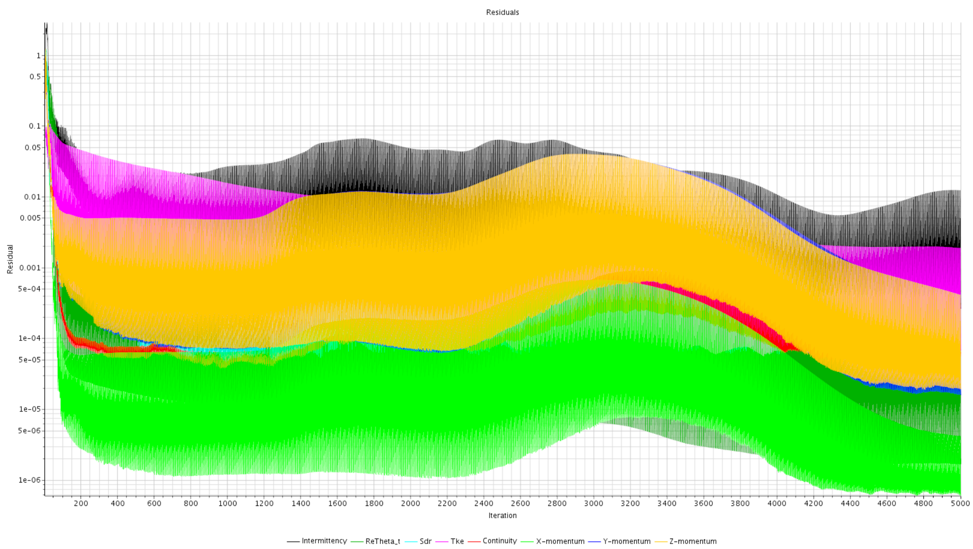

Figure 6.5: Solution Convergence for an Unsteady Configuration

In the interest of being thorough and purely for the sake of comparison, another simulation is performed using the same configuration, except in an unsteady state. Figure 6.5 reveals what the residuals look like for this type of continua.

The plots for the thrust and torque monitors from the steady simulation are given in Figures 6.6 and 6.7, respectively. Both plots exhibit an initial instability within the first 50 iterations, corresponding to the simulation residuals in Figure 6.4.

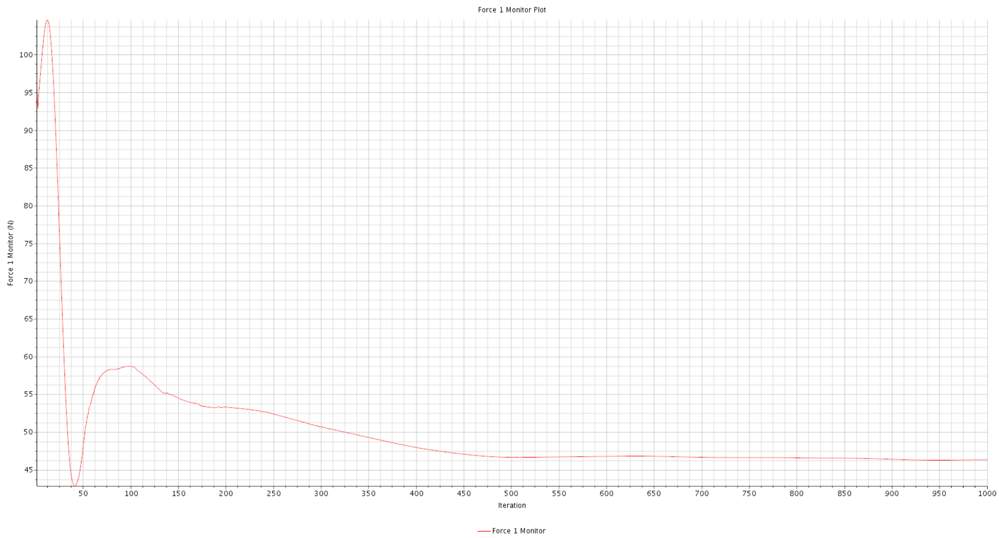

Figure 6.6: Force Monitor plot representing Thrust

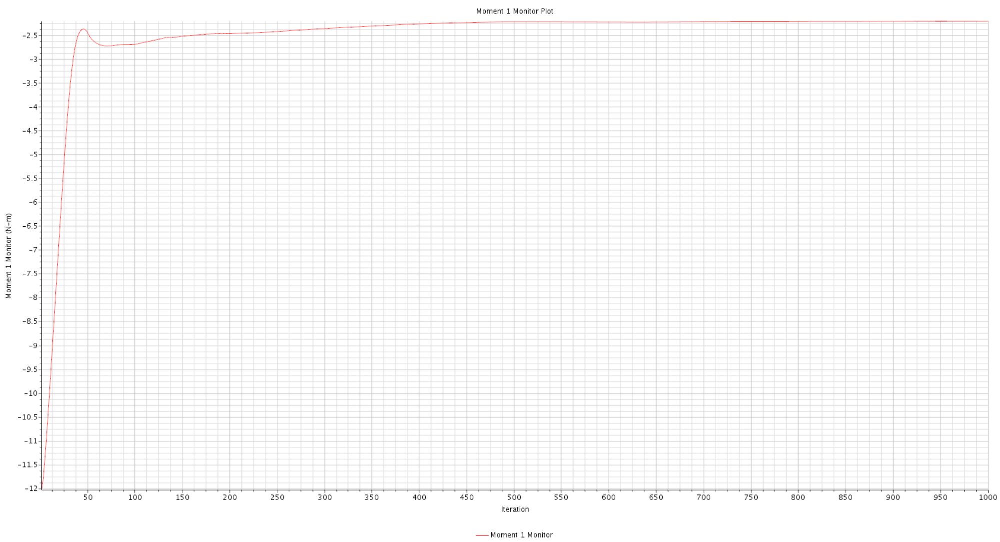

Figure 6.7: Moment Monitor plot representing Torque

6.2 Experimental Validation

In order to confirm the performance benefits of implementing a rudder bulb as well as to validate the computational setup against experimental data, a number of self propulsion tests are performed at various advance ratios. The continuum is set up as described in previous chapters, where the geometry is also processed in a similar manner. Each simulation corresponding to a design case is run for 1000 iterations, with the most important variables being recorded through the implementation of force and moment monitors.

Figures 6.8a and 6.8b depict the pressure coefficient distribution mapped onto the respective propulsive systems, with a valuable insight into the streamline behaviour in the post swirl region. The two design cases are performed at a ship speed of 20*knots*, which for the case without a rudder bulb translates to an advance ratio of 0.8968, while for the simulation incorporating the rudder bulb, the advance ratio is 0.9129.

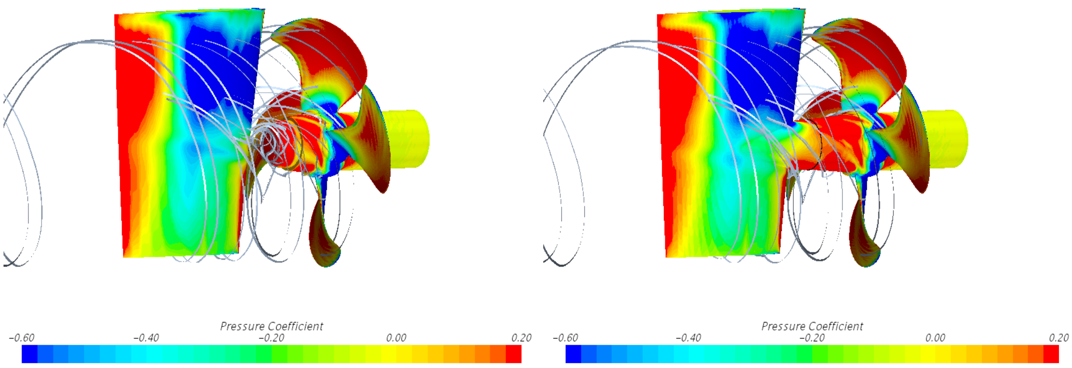

(a) Without a Rudder Bulb **(b)** With a Rudder Bulb

Figure 6.8: Starboard views of Pressure Coefficient distribution and Streamline behaviour around the Propulsion Systems

The primary objective of these simulations is to ultimately validate and verify the computational setup as well as the results produced against a set of established experimental data points. This is achieved by taking advantage of the features offered in *Matlab*, wherein the two sets of data are imported and graphed on the same set of axes for ease of comparison.

Figure 6.9 reveals the striking similarity between both plots of computational and experimental thrust and torque for the cases with and without a rudder bulb. The comparison of both sets of data is a reliable means of verification of the current model, fully validating the configuration of the continuum.

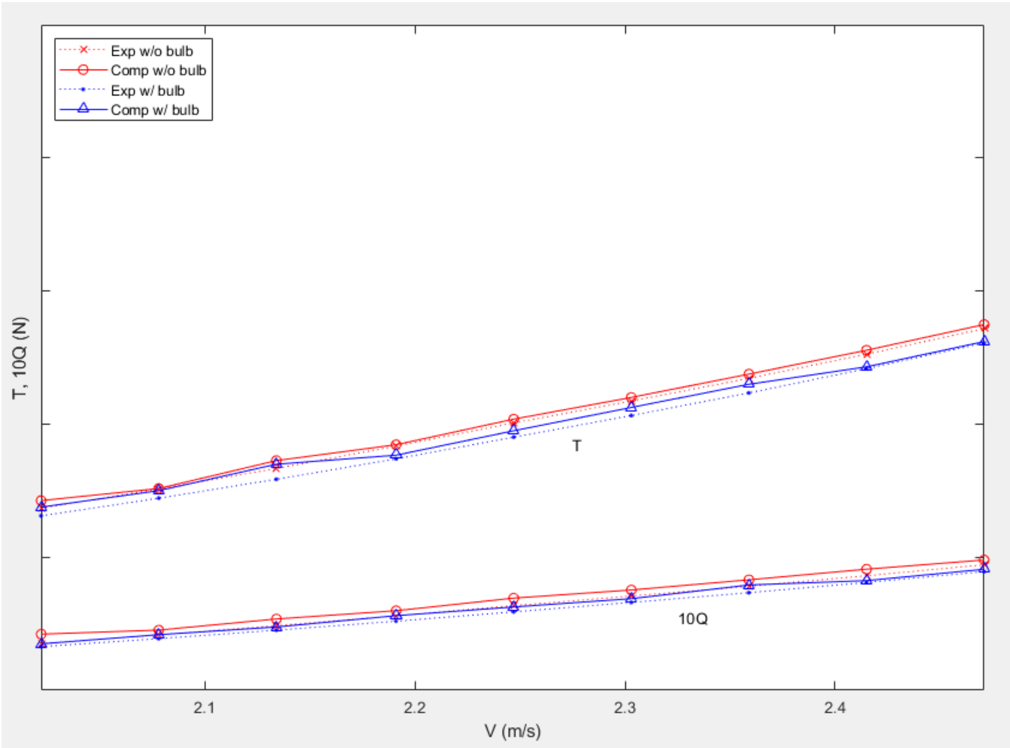

Figure 6.9: Comparison between Computational and Experimental results of Thrust and Torque

6.3 Propulsion System Optimisation

Optimising the rudder bulb further can be done in a few different ways, the most effective method being appending streamlined fins to the side of the rudder bulb. The aim is to achieve favourable influences on the propulsive performance of the system as well as gaining a more desirable flow around the rudder. Placing the fins in the rotational flow aft of the propeller triggers the generation of additional thrust in the opposite direction of the free stream motion.

The fin mesh is generated and treated in an identical manner to the mesh within the rest of the continuum. In order to ensure reliable computational results, a target cell size of 1% of the base grid size is imposed on the fins, creating an approximate addition of $300,000$ cells within the domain, depending on the scale of the fins. Each fin is then assigned an individual boundary, mirroring the blade surface settings. No additional computational resources are required to mesh and simulate geometries incorporating fins, thus the time it takes for a solution to converge is unchanged.

6.3.1 Base Case Results

Understanding the behaviour and performance of a typical propulsion system is key in determining whether the addition of rudder bulb fins has any effect on the system performance. This simulation of a plain geometry without any fins serves as a means of comparison when developing other geometries. Figure 6.10 offers a visual representation of the simulation results.

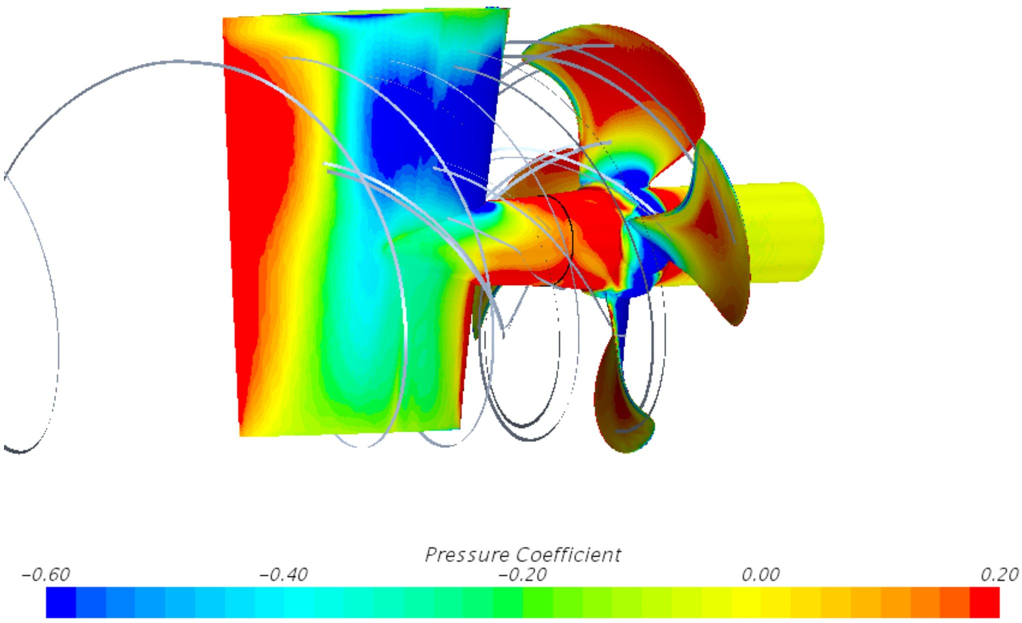

Figure 6.10: Pressure Coefficient distribution and Streamline behaviour for a typical Propulsion System

The flow in the post swirl region offers a valuable insight into what method is best in order to capitalise on its effects with an appropriate fin profile. Therefore, as an auxiliary tool to help further and better understand system performance, the monitor data is given in Table 6.2.

Table 6.2: Base Case System Performance

	Thrust	Torque
Max	46.5774	2.2075
Min	46.3232	2.2159
Sum	92.9006	4.4234
Avg	46.4503	2.2117
Coefficients	0.1707	0.0355
Efficiency	69.85%	

6.3.2 Integrated Fin Geometry Results

The process of choosing a fin profile to implement into the propulsive system geometry is an involved one. The *NACA* database offers a wide selection of various fin profiles with different characteristics. In this case, airfoil profiles are sorted by their lift characteristics since thrust is generated when the component of lift in the x-direction is greater than the drag force. Maximising the thrust or lift is what results in an enhanced system efficiency. Airfoils mainly produce drag in the direction opposite to the flow and perpendicular to the lift force.

Once the airfoils are sorted and the preferred profile chosen, the coordinates can be downloaded from the *NACA* database and imported into *Star-CCM+*, where they are converted into a solid part by means of extrusion. The chosen airfoil profile is shown in Figure 6.11.

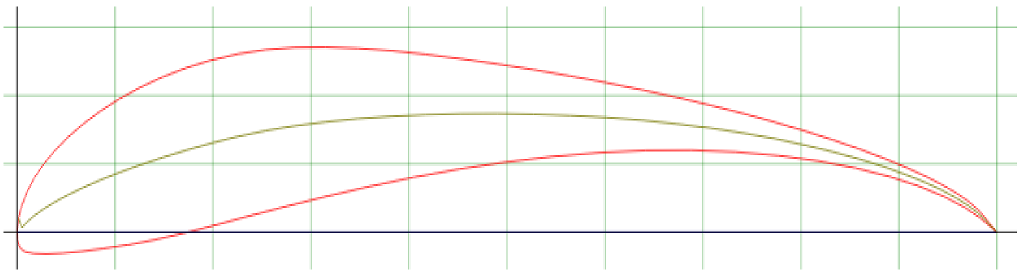

Figure 6.11: s1223-il Airfoil Profile

The s1223-il fin profile may be described as a high lift, low Reynolds number airfoil, fitting the requirements of the research objective very well. Figure 6.12 shows a graph of C_L/C_D against α for the s1223 airfoil, depicting the optimal range of angle of attack. A sensitivity study is performed and presented later in this chapter in order to determine the system performance behaviour as a function of the angle of attack of the fins.

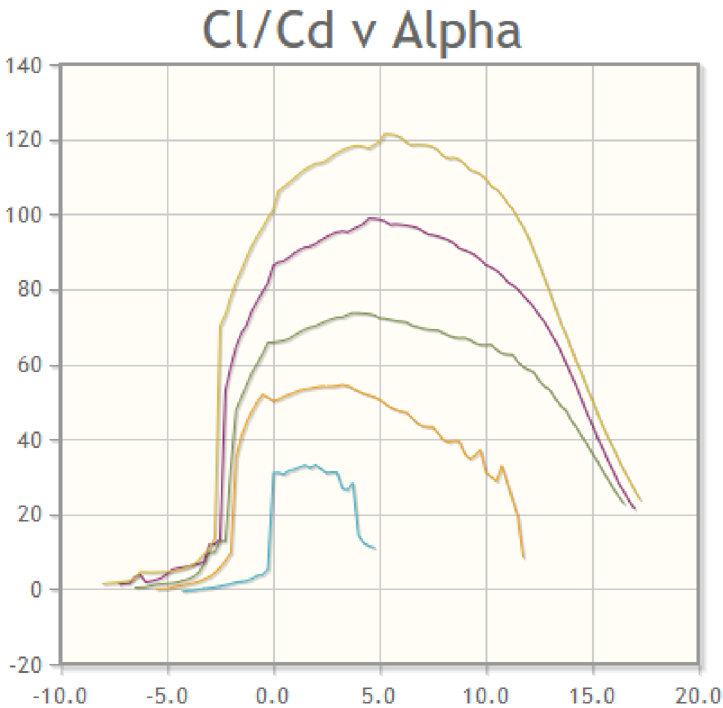

Figure 6.12: A plot of C_L/C_D vs α for s1223-il Airfoils

The geometry is identical to the base case, with the only difference of the fin on the rudder bulb being extruded to reach a span of $0.05m$. Figure 6.13 shows the results of the simulation, depicting the streamline behaviour as well as the pressure coefficient distribution for the s1223-il fin.

A number of other fin profiles with high lift characteristics, similar to the s1223-il airfoil are also tested and evaluated, using identical conditions, however, the system with s1223 fins proves to be superior in every way.

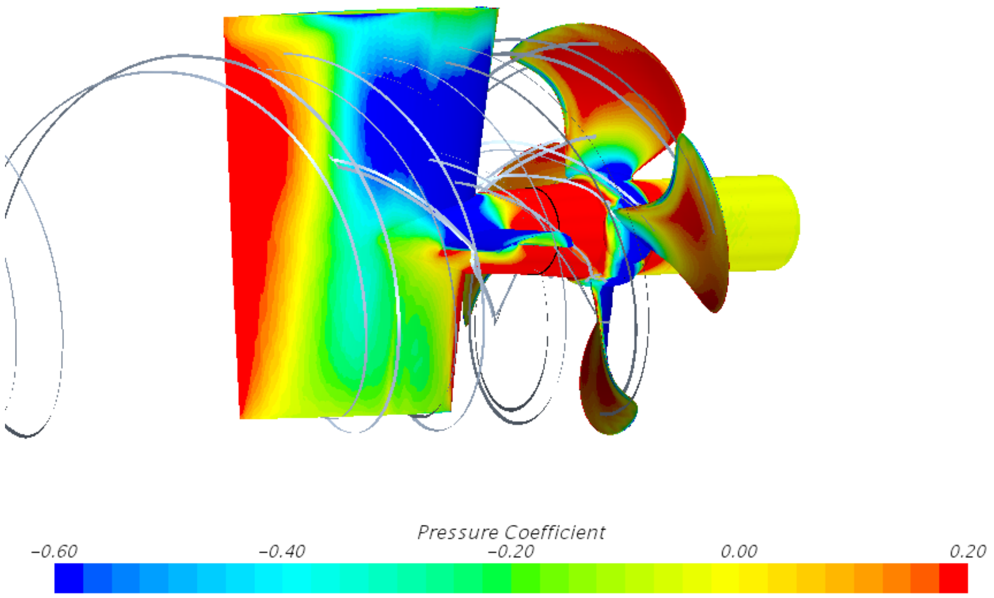

Figure 6.13: Pressure Coefficient distribution and Streamline behaviour for the s1223 Fin System

Analysing the streamlines in Figure 6.13, one can observe significantly more favourable behaviour than a plain system without fins. The data presented in Table 6.3 makes this immediately apparent.

Table 6.3: s1223-il System Performance

	Thrust	Torque
Max	47.0955	2.2264
Min	46.9886	2.230525
Sum	94.08409	4.456941
Avg	47.04204	2.228471
Coefficients	0.172927	0.035788
Efficiency	70.21%	

The s1223-il fin system has an overall efficiency of 70.21%, which is a marked improvement of 0.36% over the plain system without fins, whose efficiency comes in at 69.85%. This result is significant enough to make this geometry eligible for further optimisation and study.

6.4 Sensitivity Studies

Sensitivity analyses delve into the variation of results obtained from a mathematical model, which may be divided and assigned to particular sources of uncertainty from within the pool of inputs. The method of re-evaluating outcomes under identical conditions with slight variations in one variable, can be extremely useful in determining the most effective setup, as well as assessing the overall effect of a variable on the whole system.

6.4.1 Fin Span Sensitivity Study

The length of the fins may often be overlooked or given a lesser importance when compared to other fin characteristics, however, it may be argued that the longer a fin spans, the more thrust it generates as well as mitigating a larger area of the flow in the post swirl region. This sensitivity study aims to explore exactly the effects of the fin span on the efficiency of the propulsion system as well as the streamline behaviour.

The base case set up for comparison has a fin span of $0.05m$, therefore in order to ensure that a larger spectrum is analysed, the fin is also shortened by one increment. A number of simulations are performed in increments of $0.01m$, reaching a span that is just shy of the propeller diameter itself. The results of the simulations are given in Table 6.4.

Table 6.4: System Efficiency at different Fin Lengths

Fin Length (m)	System Efficiency (%)
0.04	70.12
0.05	70.21
0.06	70.25
0.07	70.27
0.08	70.30

The results of this study are better represented in the form of a graph, as seen in Figure 6.14. The graph is easily generated using *Matlab*, and gives a better understanding of the relationship between the length of the fins and the propulsion system efficiency.

Observing the graph reveals a distinctly positive relationship between the fin span and the efficiency, however one must not neglect the fact that an excessively long fin could tarnish the manoeuvrability of the vessel or perhaps even create physical interference with the propeller blades.

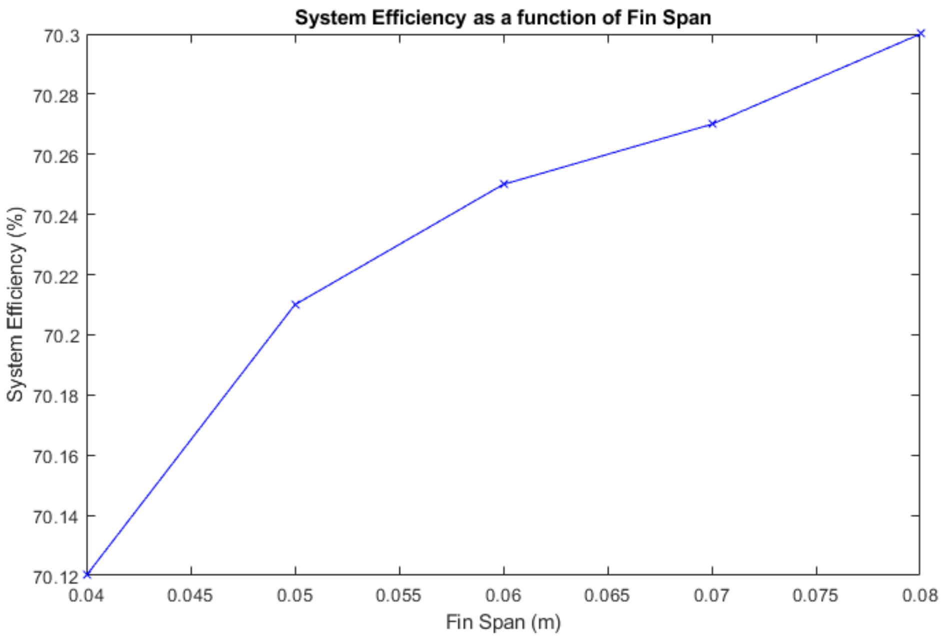

Figure 6.14: A graph of the relationship between Fin Length and System Efficiency

Choosing a fin length that is too large could result in limited articulation of the rudder, thus in the interest of retaining such features, a compromise must be reached. Therefore, all further analysis and sensitivity studies are performed using a fin length of $0.06m$. This translates to an efficiency of 70.25% which increases the difference between this system and one without any fins to 0.4%.

Figure 6.15 gives a pictorial representation of the pressure coefficient distribution and the streamline behaviour in and around the rudder assembly for this design case.

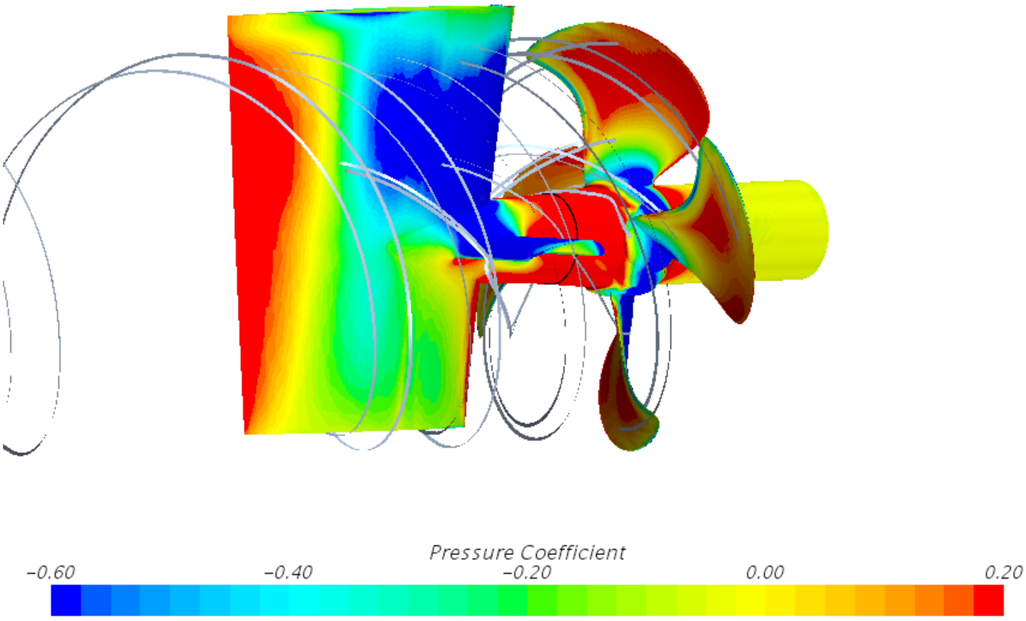

Figure 6.15: Pressure Coefficient distribution and Streamline behaviour for a Fin of 0.06m span

6.4.2 Angle of Attack Sensitivity Study

The angle of attack of the fins is another defining characteristic worthy of attention. This variable has the potential to greatly affect the performance of a propulsion system in a positive manner, therefore it is tested rigorously in the following section. A number of different simulations are performed in increments of 5°, from $-10°$ to 20°, in order to properly assess the relationship between the angle of attack and the overall system efficiency.

The results of the simulations preformed are presented below in Table 6.5. It is worth noting that the angle measured is relative to the rotational inflow from the propeller.

Table 6.5: System Efficiency at different Angles of Attack

Fin Angle (°)	System Efficiency (%)
-10	70.26
-5	71.03
0	72.51
5	73.19
10	72.84
15	72.37
20	71.63

Matlab is once again used to graph the results obtained, allowing for a much better understanding of how the performance changes as a function of the angle of attack of the fins. Figure 6.16 is a pictorial representation of the results given in Table 6.5.

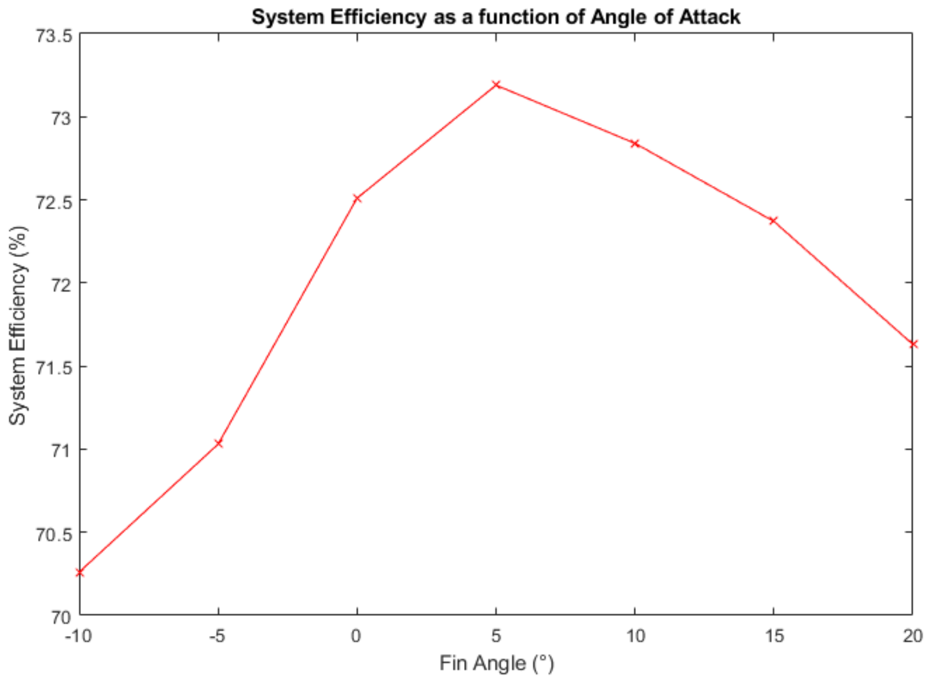

Figure 6.16: A graph of the relationship between Angle of Attack and System Efficiency

It is immediately apparent from analysing the graph that the system efficiency is proportional to the angle of attack, with significant improvements in overall efficiency to the tune of up to 2.9%. The graph shows the optimal angle of attack to be 5°, which is in line with the theoretical behaviour of s1223-il fins presented in Figure 6.12.

Figure 6.17 shows the pressure coefficient distribution mapped onto the geometry along with the favourably improved streamline behaviour in and around the post swirl region.

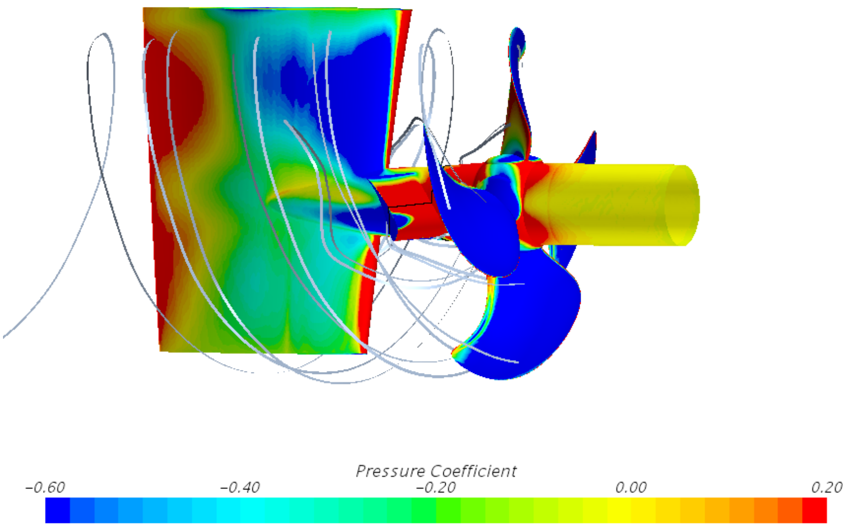

Figure 6.17: Pressure Coefficient distribution and Streamline behaviour for a 5° Angle of Attack Fin

6.4.3 Fin Placement Sensitivity Study

The purpose of this sensitivity study is to determine the ideal positioning for the fin profiles, if the geometry were to be limited to one airfoil, due to reasons related to economic feasibility, vessel downtime or otherwise.

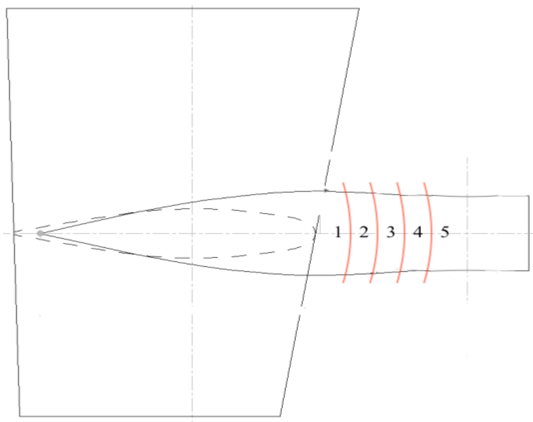

Figure 6.18: Schematic Diagram for the Fin Position Sensitivity Study

The starboard profile of the rudder bulb is split into a number of sections where a fin with the following specifications is tested; a span of 0.06m and an angle of attack of 5°. The angle of attack is kept constant regardless of where it is placed in order to preserve the ability to compare the effect of the fin placement itself. Figure 6.18 gives a better understanding of how the following simulations are performed.

Table 6.6: System Efficiency at different Fin Positions

Section	System Efficiency (%)
1	73.13
2	73.19
3	73.47
4	73.93
5	74.84

Analysing the results of this sensitivity study proves extremely insightful, as the position of the fins plays a significant role in the amount of additional thrust they generate. Sections four and five both produce the highest performing scenarios with efficiencies at least 4.9% higher than the base case without any fins. However, it is important to keep manoeuvrability in mind when testing fins with a span of 0.06m in sections one to four, since rudders typically need to articulate at least $\pm 60°$ from the neutral axis.

Positioning the fins on the fixed part of the bulb, after the steering clearance, eliminates any issues of manoeuvrability and tends to improve the system performance, therefore the setup with the fins in section five, shown in Figure 6.19, proves to be doubly advantageous.

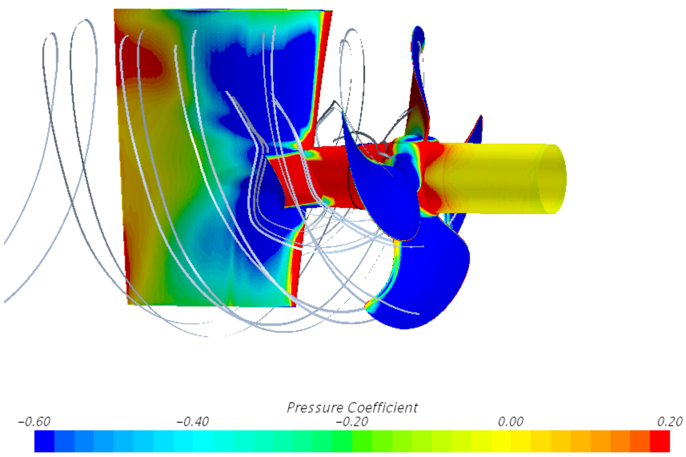

Figure 6.19: Pressure Coefficient distribution and Streamline behaviour for a fin setup in Section 5

6.5 Fin Stacking

The analysis of the various fin properties in the sensitivity studies allows a deeper understanding of the behaviour of individual fins. Despite the results of the simulations all proving to be extremely positive, adding multiple fins to the rudder geometry has the potential to increase the gains in efficiency observed previously. This section explores the various configurations evaluated in search of an optimal design with truly significant improvements.

A number of various fin arrangements are set up for testing and simulation in order to attempt to compute as many combinations with great potential as possible. This area of research could take a significant amount of time, therefore in the interest of efficiency, only a few combinations that have the potential to increase the system efficiency by a significant amount are simulated. The following section presents two of the most successful simulations.

6.5.1 Four Fin Configurations

The previous research establishes the optimal values for each of the most important variables studied. This allows for a more knowledgeable approach when determining the configurations to simulate and test when attempting to improve the system efficiency. The best performing setup consists of two fins aligned with the rotational inflow from the propeller, with an angle of 5°, located approximately $0.002m$ from the steering clearance.

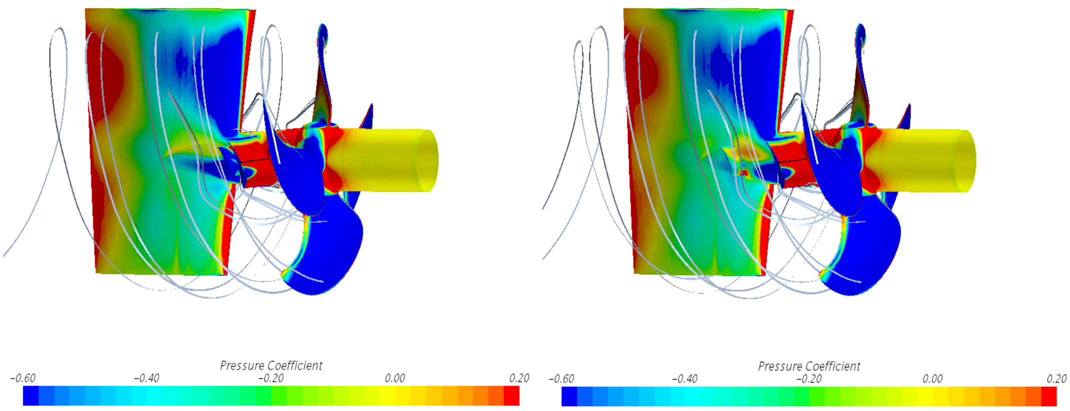

(a) Close Configuration

(b) Distant Configuration

Figure 6.20: Pressure Coefficient distribution and Streamline behaviour for two configurations involving two sets of fins

The configurations presented in Figure 6.20, maintain the setup described previously while making use of an additional set of similar fins that are scaled down by a particular factor and placed in different positions. Figure 6.20a depicts the smaller, scaled down set of fins at a distance of $0.02m$ from the original fins, while Figure 6.20b shows the latter configuration with the smaller set of fins situated on the rudder.

Each configuration proves to be significantly more efficient than a setup without any fins, however the system efficiency achieved is not enough to warrant the extra cost of installing an additional pair of fins. This is especially true when comparing the system efficiency with the results obtained from the setup presented in Figure 6.19. The results for the close configuration and the distant configuration are given in Tables 6.8 and 6.9, respectively.

Table 6.7: Results of Four Fin Configurations

Table 6.8: Close Configuration

	Thrust	Torque
Max	57.4625	2.5533
Min	57.4285	2.5522
Sum	114.891	5.1055
Avg	57.4454	2.5527
Coefficients	0.2117	0.0409
Efficiency	74.84%	

Table 6.9: Distant Configuration

	Thrust	Torque
Max	57.5078	2.5530
Min	57.4569	2.5551
Sum	114.964	5.1082
Avg	57.4823	2.5541
Coefficients	0.2113	0.0410
Efficiency	74.85%	

While the close configuration, with an efficiency of 74.84% matches the efficiency of the best performing setup, the distant configuration has an efficiency of 74.85%. Albeit an increase, the improvement in system efficiency through the introduction of the second set of fins, is only of 0.01%, which is simply not enough to justify the expense of purchasing and retrofitting such a system.

A number of various configurations that differ greatly in geometry are also tested, in order to investigate as many setups as possible, however, all fall short of the configuration described in Section 6.4.3. As a result, the following section is based exclusively on that geometry.

6.6 Off-Design Instances

This section is dedicated to evaluating certain instances when the vessel is not operating at a cruising speed of 20*knots*, which corresponds to an advance ratio of 0.9129. Two simulations are set up to analyse the performance of the vessel when it is sailing above or below the typical operating conditions. The upper limit for the off-design test case is defined by an advance ratio of 0.9348, while the lower limit is defined using an advance ratio of 0.8904, translating to higher and lower ship speeds, respectively.

The two individual simulations are based on the design and geometry detailed and described in Section 6.4.3 as no significant improvements in system efficiency are made using multiple sets of fins. As a form of reference, the efficiency at constant operating conditions is given as 74.84%. The results of both cases are given in Figures 6.21a and 6.21b, showing the differences in pressure coefficient distribution as well as streamline behaviour for ship speeds below and above operating conditions, respectively.

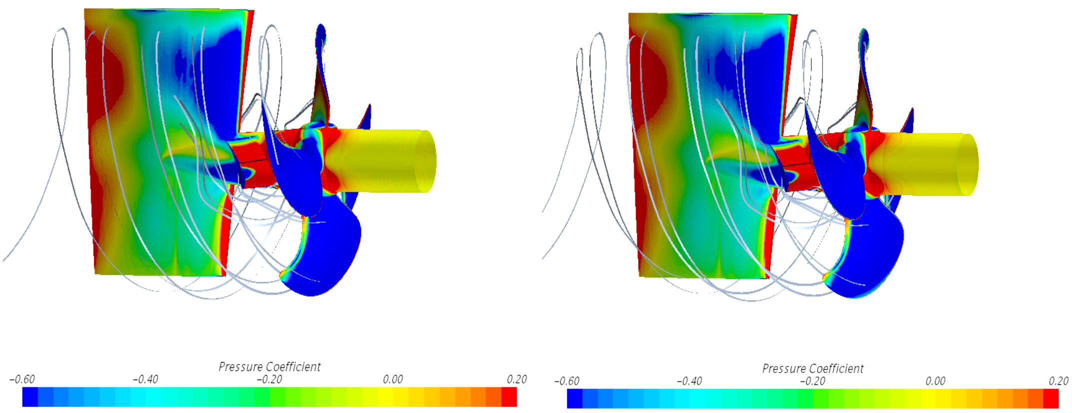

(a) Lower Limit

(b) Upper Limit

Figure 6.21: Pressure Coefficient distribution and Streamline behaviour for Off-Design Cases

It is evident from comparing the two figures, that the pressure coefficient distribution is slightly more favourable when operating at a lower ship speed. The streamlines are observed to be somewhat superior too. This is unanimous with the results obtained from the force and moment monitors, since the lower limit case has an efficiency of 75.77%, while the upper limit case has an efficiency of 73.89%. This reveals that the vessel loses efficiency when sailing at a higher ship speed, and gains efficiency while sailing slightly below cruising speed. This is true until reaching an advance ratio of 0.3814, after which the efficiency starts to decrease.

7 Discussion

The sensitivity studies performed all contribute towards forming a more holistic understanding of the effects of energy saving devices and how their influence affects the flow within the post-swirl region. The research is based solely on fins of an s1223-il profile, as this profile was determined to achieve the best results.

There are a number of fin characteristics one may choose to investigate, however the ones studied in this report are considered to bear the most significance and potential when it comes to achieving a better performing propulsive system. The placement sensitivity study may also be related to the rudder geometry itself, however this introduces a number of limitations as discussed in Appendix A.

The best performing configuration is the one incorporating opposite fins at an angle of attack of 60° at a distance of $0.002m$ from the steering clearance. The span of both fins is $0.06m$. The port side profile faces upwards as one would expect an airfoil to be oriented, while the starboard side profile is placed upside down, to better suit its inflow. The system efficiency of such a setup is 74.84%, which is a significant improvement of 4.99% over the base case without a fin geometry.

Despite further efforts to improve the aforementioned system efficiency, configurations with multiple sets of fins, placed close to the original fins or farther away provided no additional thrust. As a result, most configurations performed much worse than the previously described setup. One particular configuration has an efficiency of 74.85%, however, this was not enough to justify the extra cost an entity would incur to install such a configuration. The following section delves deeper into the benefits and costs involved in incorporating the optimal fin layout.

7.1 Cost Benefit Analysis

This section offers a simplistic approach for weighing up the costs and benefits of retrofitting the rudder bulb fins onto an operational vessel. A cost benefit analysis is a simple tool used to evaluate the costs and benefits of a project, whose results determine a payback period for the investment.

The costs of implementing an ESD of this description are given in the list below:

- Initial purchase,
- Installation,
- Maintenance,

- Vessel downtime.

It is also necessary to assign a monetary value to the costs listed above. Estimates within literature point to such a task costing an entity approximately €500,000 [15].

The benefits of implementing the described ESD are given as follows:

- Improved vessel efficiency,
- Reduced fuel consumption,
- Short return on investment,
- Reduced vessel emissions.

In order to assign a monetary value to the benefits, similar values to those presented in the Article titled 'Fuel Costs in Ocean Shipping' [16] are assumed. Therefore, the expenses saved on fuel by introducing the ESD equate to approximately €40,000,000 per year. Assuming a 5% reduction in fuel consumption the payback time may be evaluated using the following expression:

$$\frac{total\ cost\ of\ implementation}{total\ benefits\ (revenue)} = length\ of\ payback\ period \tag{7.1}$$

Using the relationship in Equation 7.1, the length of the payback period is given as 3 months.

8 Conclusion

This research project focuses on the development of a CFD model of a marine application propulsion system that includes rudder bulb fins as the primary energy saving device in the post-swirl region. The majority of the research is centred around the evaluation of the most important fin characteristics, with a dedicated focus on increasing the overall system efficiency. The investigation of various fin parameters along with their influence on the system performance, allows for the optimal rudder bulb fin topology to be established.

The two previous chapters serve as an intensive, thorough presentation and discussion of the results obtained. The primary goal of this research project, that of determining the optimal topology of the rudder bulb fins, is achieved in the form of a two fin setup, both aligned with the rotational inflow, reaching a system efficiency improvement of 4.99% over a system without any fins. Testing other configurations with multiple sets of fins does not yield any worthwhile improvements that are significant enough to warrant the cost of an extra set of fins.

The results show the benefits of the developed optimised topology, which is able to maximise system efficiency with minimal modifications and capital expenditure. While the optimised geometry improves the system performance by $\approx$ 5%, this does not mean it would offer the same benefits for all vessels, since each hull design and propeller result in a different flow pattern. However, the same approach and methodology can be applied to other energy saving devices and case studies, meeting the specific requirements of other vessels.

8.1 Future Work

This section explores possible avenues of research that may be carried out in the future in order to add to the work that has already been done to date. In the interest of driving the margin of efficiency improvement even higher, there are a number of other variables to investigate, which have the potential to improve the promising results achieved thus far.

The parameters investigated in this research project are considered to bear the most weight in terms of potential to improve the system efficiency, however, there are a number of other variables to consider when determining which combination to employ in order to achieve the best results possible. Parameters such as chord distribution and twist could both be investigated in detail in order to grow the understanding of the influence of such characteristics.

Therefore, it may be worthwhile to develop a multi-objective approach to optimisation that can be used to establish a geometry that is able to recover energy losses by mitigating the resulting rotational flow from the propeller. The use of multiple fins is also an extremely vast and sensitive area of research that given enough time, could prove to have significant potential to introduce a level of control over the flow in the post swirl region and even increase the system efficiency further.

References

[1] International Maritime Organisation. URL: http://www.imo.org/en/OurWork/Environment/PollutionPrevention/AirPollution/Pages/Default.aspx.

[2] International Maritime Organisation. *Energy Efficiency Measures*. URL: http://www.imo.org/en/OurWork/Environment/PollutionPrevention/AirPollution/Pages/Technical-and-Operational-Measures.aspx.

[3] John S. Carlton. *Marine propellers and propulsion*. Butterworth-Heinemann, 2012.

[4] Fathom Shipping. *Propeller Technology to Make Your Ship More Efficient*. Oct. 2013. URL: https://gcaptain.com/propeller-technology-ship-efficient/.

[5] Takafumi Kawamura, Kazuyuki Ouchi, and Takeo Nojiri. "Model and full scale CFD analysis of propeller boss cap fins (PBCF)". In: *Journal of marine science and technology* 17.4 (2012), pp. 469–480.

[6] YOSHIHISA Okada et al. "The development of "Ultimate Rudder" for EEDI". In: *Proceedings of International Conference on Computational Methods in Marine Engineering Rome Italy*. 2015.

[7] Hans Buch. *Rudder design and supply*. Sept. 2017. URL: https://hansbuch.dk/marine/rudder-and-steering-gear-service/rudder-design-and-supply.

[8] Kawasaki Heavy Industries. *Energy-saving Technology*. 2018. URL: http://global.kawasaki.com/en/mobility/marine/technology/energy_saving.html.

[9] Jialun Liu and Robert Hekkenberg. "Sixty years of research on ship rudders: effects of design choices on rudder performance". In: *Ships and offshore structures* 12.4 (2017), pp. 495–512.

[10] Shin Keun Woo and Andersen Poul. "CFD Analysis of Rudder Bulb Performance in Ship Manoeuvring". In: ().

[11] Keun Woo Shin, Ege Lundgren, and Jens Ring Nielsen. "CFD-based optimization of rudder bulb systems". In: *Proceedings of World Maritime Technology Conference Saint-Petersburg, Russia*. 2012.

[12] Singiresu S Rao. *Engineering Optimization: Theory and Practice Fourth Edition. sJohn Wiley and Sons*. 2009.

[13] URL: https://ittc.info/.

[14] Shen Hai-long, Enock Omweri Obwogi, and Su Yu-min. "Scale effects for rudder bulb and rudder thrust fin on propulsive efficiency based on computational fluid dynamics". In: *Ocean Engineering* 117 (2016), pp. 199–209.

[15] URL: https://glomeep.imo.org/technology/propulsion-improving-devices-pids/.

[16] *Fuel Costs in Ocean Shipping*. 2020. URL: https://www.morethanshipping.com/fuel-costs-ocean-shipping/.

A Appendix

A.1 Rudder Fins Tests

The purpose of this experimentation is to determine whether placing fins on the rudder is a viable option and if it produces any worthwhile results.

The starboard profile of the rudder is split into four quadrants where a fin with the following specifications is tested; a span of $0.06m$ and an angle of attack of 5°. The angle of attack is however, not optimised according to which quadrant it is part of. This is done in order to preserve the ability to compare the effect of the fin placement itself.

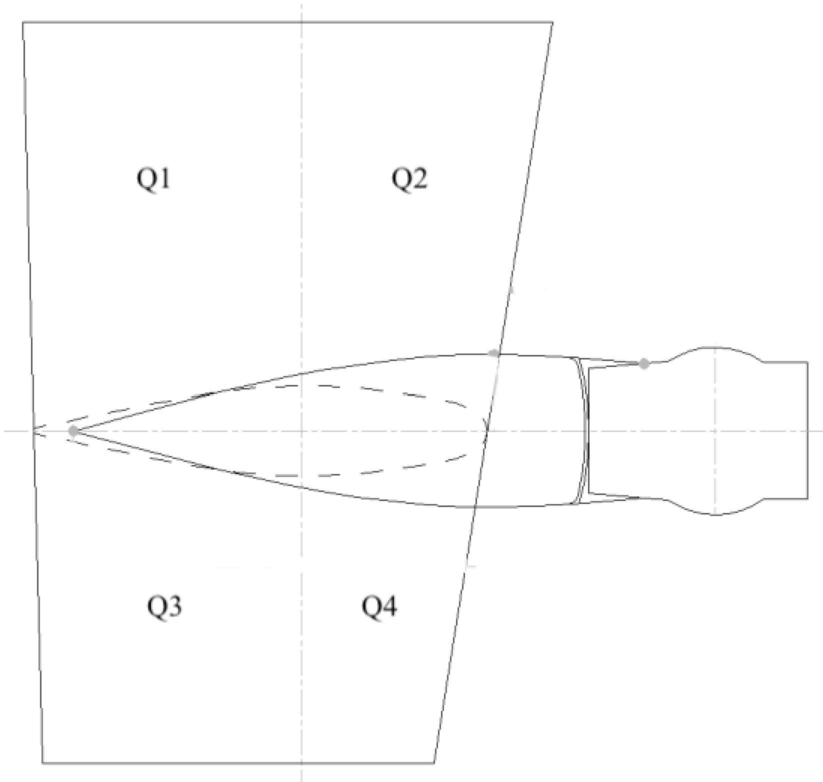

Figure A.1: Schematic diagram of the Rudder Quadrants

Figure A.1 shows the quadrants, where for each simulation, the fin geometry is translated to the middle of the quadrant. The results for each computation are presented in Table A.1, where the left column corresponds to the numbering within the schematic diagram.

Table A.1: System Efficiency at different Fin Positions

Quadrant	System Efficiency (%)
Q1	70.31
Q2	71.16
Q3	70.44
Q4	71.29

Analysing the results of this sensitivity study proves extremely insightful, as the placement of the fins plays a major role in the amount of additional thrust they generate. Quadrants one and three are only marginally more efficient than a system without any fins. On the other hand, the fin within quadrant four produces a system efficiency of 71.29%, which is considerably higher than a geometry without fins. In fact, it is 1.44% more efficient than the base case.

The best and worst performing fin configurations are shown in Figures A.2a and A.2b serve as a means of comparison between the best and worst performing configurations. Both figures map the pressure coefficient distribution onto the geometry while visualising the streamlines in the post swirl region.

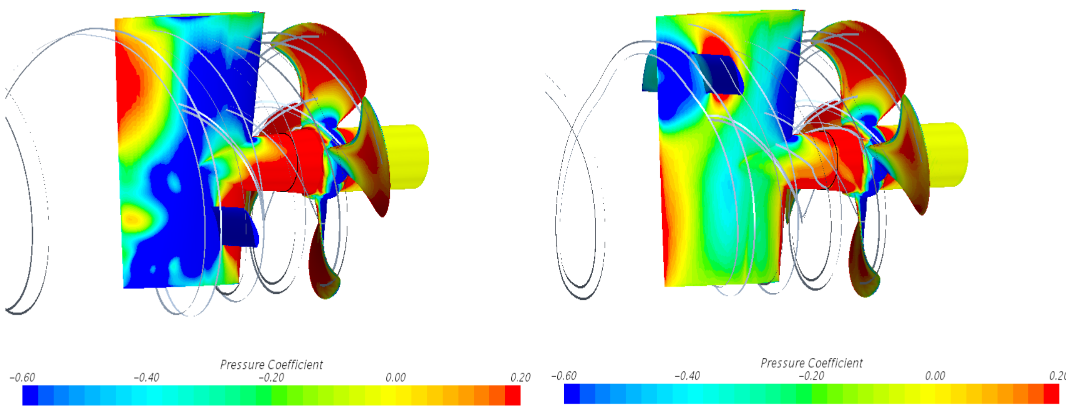

(a) Fins in Q4

(b) Fins in Q1

Figure A.2: Starboard views of Pressure Coefficient distribution and Streamline behaviour in Q4 and Q1

Observing and comparing the two figures in further detail reveals that placing the fin in Q4 decreases the surface pressure coefficient on the rudder while placing it in Q1 increases it. The streamline behaviour around the rudder is similarly much more favourable in Q4 when compared to Q1.

Once the optimal location is determined, another set of fins is introduced in order to investigate the effect of multiple fins on the overall system efficiency. Figure A.3 depicts the results of a setup using two fins.

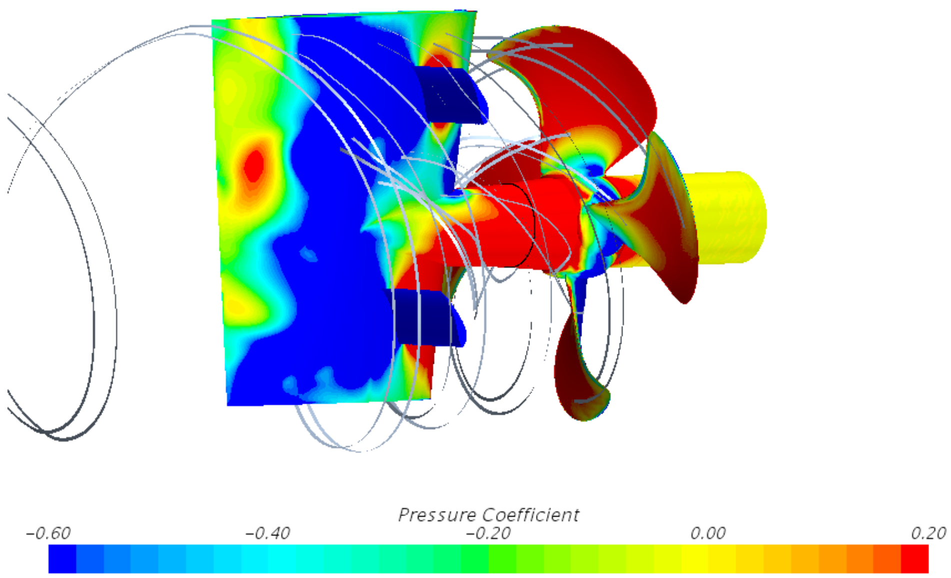

Figure A.3: Pressure Coefficient distribution and Streamline behaviour with Fins in Q2 and Q4

This configuration has an efficiency of 72.46%, however, despite presenting an improvement of 2.61% over the base case without any fins, introduces a number of potential issues and limitations, which is why this section is very experimental.

A.2 Limitations

There are a few considerations to keep in mind when investigating fins positioned on the rudder itself. These limitations are significant reasons why such configurations are typically not considered. The limitations are as follows:

- Decreased manoeuvrability,
- Introduction of bending moments,
- Introduction of forces,
- Increased stresses.